Available online at www.sciencedirect.com

ScienceDirect

Geochimica et Cosmochimica Acta 294 (2021) 315–334

Geochimica et Cosmochimica Acta

www.elsevier.com/locate/gca

High-resolution, long-term isotopic and isotopologue variation identifies the sources and sinks of methane in a deep subsurface carbon cycle

Oliver Warr [a,*], Edward D. Young [b], Thomas Giunta [a], Issaku E. Kohl [b], Jeanine L. Ash [b], Barbara Sherwood Lollar [a]

[a] Department of Earth Sciences, University of Toronto, Toronto, Ontario, Canada
[b] Department of Earth, Planetary and Space Sciences, University of California Los Angeles, Los Angeles, California, USA

Received 5 August 2020; accepted in revised form 5 December 2020; available online 15 December 2020

Abstract

This study applies a combined isotope and doubly-substituted isotopologue ('clumped') methane approach to samples collected over a 9-year long-term experiment at the Kidd Creek scientific observatory located 2.4 and 2.9 km depth below surface, combined with previously published data from 2.1 km below surface. The observatory is located in a fractured rock system within Kidd Creek Mine in Timmins, Ontario, Canada, situated within a 2.7 Ga Volcanogenic Massive Sulphide (VMS) deposit on the Canadian Shield. Isotope and isotopologue methane data suggest a temporal variation in the various sources of methane within the fracture fluids system between 2.1 and 2.9 km below surface. Predominantly abiogenic methane is identified in samples collected from the deepest level of the mine (2.9 km). Comparing new data from the 2.4 km level with previous data from 2.1 km suggests addition of a small component of microbially-generated methane to the fracture water systems at 2.4 km. The temporal evolution of the methane isotopologue signatures suggest an additional process is occurring within these waters. Specifically, methane in samples from 2.4 km (and some from 2.9 km) approach low-temperature thermodynamic equilibrium in clumped isotopologue space, which is not consistent with kinetically-controlled methane production (either microbial or abiogenic). Anaerobic Oxidation of Methane (AOM) during microbial methanotrophy is shown to be the most likely process to drive such re-equilibration via isotopic bond re-ordering. This study provides an unprecedented high-resolution temporal record over more than a decade for methane in a deep subsurface crystalline environment and demonstrates the advantages of clumped isotopologue studies to identify multiple processes controlling the methane cycle in these systems including both abiotic and biotic methane production and methanotrophy.

Keywords: Methane; Clumped isotopologues; AOM; Microbial methanogenesis; Deep biosphere

1. INTRODUCTION

Within crystalline rocks of the Precambrian crust, methane is frequently present as a major gas component dissolved in saline fracture waters and has been identified globally in sites from the Canadian Shield, to the Fennoscandian Shield and South Africa Craton (Sherwood Lollar et al., 1993a, 2008; Ward et al., 2004; Kietäväinen and Purkamo, 2015; Drake et al., 2017). Methane in such environments has been postulated to be generated either abiogenically through water–rock interactions via the Sabatier-type reaction, or through microbial

☆ DOI of original article: 10.1016/j.gca.2020.11.026.
* Corresponding author.
E-mail address: oliver.warr@utoronto.ca (O. Warr).

https://doi.org/10.1016/j.gca.2020.12.002

methanogenesis. Once formed, methane can subsequently be affected by processes such as mixing/addition of secondary methane, as well as through microbial activity such as methanotrophy (Ward et al., 2004; Sherwood Lollar et al., 2006; Etiope and Sherwood Lollar, 2013 and references therein). The crystalline Precambrian crust accounts for approximately 72 % of the total surface area of the continents and over 80 % of terrestrial crust at depths below 2 km (Goodwin, 1996; Gleeson et al., 2016). Sherwood Lollar et al. (2014) demonstrated that these regions of ancient crust are still geochemically active, with global hydrogen production in the deep crystalline basement comparable to that of the marine lithosphere. This was further reinforced by the work of Parnell and Blamey (2017) and, more recently, Warr et al. (2019) who independently confirmed that the ancient basement could serve as a major source of H_2, a key reactant sustaining subsurface methane production via both abiotic and microbial reactions (e.g. Sherwood Lollar et al., 1993b, 2002, 2006). Considering the global crustal volumes involved along with the potential for hydrogen production and conversion to methane, these multiple lines of investigation suggest abiogenic methane production in both marine seafloor and terrestrial crystalline rock environments represents a significant, yet still poorly constrained, reservoir in the global carbon cycle (Klein et al., 2019; Warr et al., 2019).

1.1. Rare isotopologues of methane

Recently, it has become possible to analyse low abundance isotopic species of methane (rare isotopologues) beyond those used for traditional isotope-based studies (i.e. $^{12}CH_4$, $^{13}CH_4$ and $^{12}CH_3D$). These naturally occurring low abundance isotopologues, which in total represent less than 0.0006 % of all methane species, contain one or more additional heavy isotopes (i.e. ^{13}C or D) to those used in conventional isotope analyses, and are usually referred to as 'clumped' or 'doubly substituted' isotopologues (Stolper et al., 2014b; Ono et al., 2014; Young et al., 2016; Douglas et al., 2017). Through measurement of the most abundant of these multiply-substituted isotopologues ($^{13}CH_3D$), studies have demonstrated that when methane forms at thermodynamic equilibrium, the relative abundance of $^{13}CH_3D$ changes as a function of temperature, as predicted by Wang et al. (2004), Ma et al. (2008) and Webb and Miller (2014) and others. This results in equilibrated methane produced at progressively lower temperatures having increasingly higher proportions of $^{13}CH_3D$ than would be predicted based on a random (stochastic) distribution of the constituent isotopes (Stolper et al., 2014a, 2014b; Ono et al., 2014; Young et al., 2016; Eldridge et al., 2019). The measured abundance of $^{13}CH_3D$ relative to the stochastically predicted amount is typically denoted using the Δ notation and is expressed in ‰ (Wang et al., 2004; Eiler, 2007). The temperature-Δ relationship is the basis for the application of this rare isotopologue as a geothermometer to provide constraints on methane production temperatures in a variety of natural settings (e.g. Stolper et al., 2014a, 2014b, 2015; Wang et al., 2015; Douglas et al., 2017; Young et al., 2017; Wang et al., 2018, Thiagarajan et al., 2020a). However, relying on the relative abundance of $^{13}CH_3D$ alone to determine formation temperature can be misleading due to kinetic effects associated with microbial methanogenesis pathways (Stolper et al., 2014a, 2015; Wang et al., 2015; Young et al., 2017; Gruen et al., 2018; Ash et al., 2019; Giunta et al., 2019; Young, 2019, Gropp et al., in press; Ono et al., 2021). This can result in unrealistically high apparent temperatures being calculated from $\Delta^{13}CH_3D$ for natural samples and laboratory cultures (e.g. Wang et al., 2015; Douglas et al., 2017; Young et al. 2017; Gruen et al., 2018; Giunta et al., 2019).

Recently, the ability to accurately resolve and measure the next most abundant doubly-substituted isotopologue ($^{12}CH_2D_2$) can be combined with $\Delta^{13}CH_3D$ to plot a thermodynamic equilibrium line in isotopologue space (Young et al., 2016, 2017). Thermogenic methane formed through the thermal decomposition of organic material is typically observed to lie on this equilibrium line (Stolper et al., 2014a, 2014b, 2015; Young et al., 2016, 2017), although recently some exceptions to this have been noted in laboratory experiments (Shuai et al., 2018) and in theoretical models of methane production (Xia and Gao, 2019). In instances where methane does not plot on the $\Delta^{13}CH_3D$-$\Delta^{12}CH_2D_2$ equilibrium line, the suggestions are that this methane formed out of equilibrium through kinetically driven processes such as the abiotic Sabatier reaction or via microbial activity; or under some conditions via pyrolysis of organic material under (Xia and Gao, 2019). Alternatively, methane may have been affected by additional processes which affect the overall isotopic composition e.g. mixing of multiple components (Young et al., 2016, 2017).

1.2. Kidd Creek Observatory for investigation of the deep terrestrial carbon cycle

Kidd Creek Observatory on the Canadian Shield has, over the past 2 decades, provided an unprecedented long-term monitoring and investigative setting more than 2 km below surface in the continental lithosphere for investigation of the preservation of deep fluids, water–rock reaction driven habitability, subsurface microbial life (Lollar et al., 2019) and developments of frameworks for deciphering the origin of methane (Etiope and Sherwood Lollar, 2013 and references therein). While not a pure abiotic end-member, a series of studies have suggested an important role for abiotic organic synthesis in the production of CH_4 and higher alkanes (ethane, propane, butane) (Sherwood Lollar et al., 2002, 2006, 2008), and H_2 production by serpentinization (Sherwood Lollar et al., 1993a, 1993b, 2014; Warr et al., 2019). Further, radiolytic processes related to the highly radiogenic environment have been shown to not only produce additional H_2 from radiolytic decomposition of water, but to produce dissolved SO_4 by indirect radiolytic oxidation of the pyrite and reduced sulfur minerals (Li et al., 2016). Cell counts and culture-based methods (Most Probable Number analysis) have recently demonstrated the presence of H_2– utilizing and alkane-oxidizing SO_4 reducing bacteria in the Kidd Creek fluids (Lollar et al., 2019), but the low cell concentra-

tions suggest rates of microbial activity are low, consistent with observations in other deep subsurface communities in both deep continental (Lin et al., 2006; Magnabosco et al., 2018a) and oceanic subsurface ecosystems (Trembath-Reichert et al., 2017; NASEM, 2018). To investigate questions at the intersection of abiotic organic synthesis and life, we require environments that are not beyond the thermal (or other) limits to life, but where abiotic processes may still occur at significant enough rates, or even if slow rates prevail, where preservation of the products of such reactions is significant enough that "abiosignatures" can be identified and where the abiotic cycle and biological carbon cycle co-exist. As such the Kidd Creek system provides a compelling setting for examining how clumped methane isotopologues can address questions on the rates, mechanisms and processes of deep subsurface methane formation and evolution in the Precambrian crust.

1.3. Carbon sources in Archean hydrothermal seafloor deposits of the Abitibi Province

Formed by regional hydrothermal processes on the Archean seafloor, the main graphite-bearing lenses at Kidd Creek are carbonaceous meta-argillites that have been extensively studied in the context of Kidd Creek and other Archean carbonaceous horizons of the Abitibi province of the Canadian Shield (Springer, 1985; Wellmer et al., 1999; Ventura et al., 2007). A comprehensive picture across the province as a whole shows overall trends of increasing total organic content (% TOC) as high as 10–15% at some sites that correlate with the most depleted $\delta^{13}C$ values for TOC – values as low as −48‰ (Wellmer et al., 1999). This correlation has been interpreted to arise in small restricted sea-floor basins where Precambrian stratified seas resulted in trapping of microbially produced CH_4 recycling isotopically "light" carbon into the sediment column due to oxidation processes (Schoell and Wellmer, 1981; Wellmer et al., 1999; Ventura et al., 2007).

With specific focus to the Kidd Creek setting though, this deposit is interpreted as a massive hydrothermal system formed in a proximal seafloor setting within a larger basin setting (Thurston et al., 2008). Here carbon sources and processes are associated with little evidence of the extreme ^{13}C-depletions attributed to methane cycling observed elsewhere in the province (Schoell and Wellmer, 1981; Wellmer et al., 1999). This is based on both the significantly more ^{13}C-enriched nature of the TOC values observed there (−18 to −33‰) and lack of correlations between TOC levels (1–10%) and $\delta^{13}C$ values. The range of $\delta^{13}C$ values for the highly graphitized and refractory TOC of Kidd Creek is similar to the range reported for Phanerozoic and even modern immature organic matter (−20 to −30‰) (Schoell and Wellmer, 1981; Clark and Fritz, 1997; Wei et al., 2018). While to our knowledge studies have not been done to compare methane generated from modern organic matter to what might be generated from an Archean carbonaceous argillite, the similarity in source material $\delta^{13}C$ values does not suggest the latter would be markedly different, in isotopic composition anyway. Hence while some contribution of thermogenic methane to the Kidd Creek gases cannot be arbitrarily ruled out, it is nonetheless clear that the Kidd Creek gases do not share carbon and hydrogen isotope signatures that overlap with conventional thermogenic gas.

These Precambrian hydrothermal seafloor systems were characterized by extensive carbonization, where hydrothermal fluids rich in CO_2 induced formation of carbonates in less reduced zones and production of graphite in more reducing (Ventura et al. 2007). As noted above, while microbial activity in Precambrian stratified small basins are believed to account for the more ^{13}C-depleted range of $\delta^{13}C$ values observed at some sites, at other sites such as Kidd Creek the prevalent graphitic horizons with more ^{13}C-enriched $\delta^{13}C$ values have been attributed to addition of hydrothermal graphite by the reaction:

$$n\mathrm{CO}_{2(\mathrm{magmatic})} + (2n + x)\mathrm{CH}_2 \rightarrow 3n\mathrm{C}^0 + 2n(\mathrm{H}_2\mathrm{O}) + \mathrm{xCH}_{2(\mathrm{hydrothermally\ altered})} \quad (1)$$

rather than generation of graphite by *in situ* dehydrogenation and aromatization of more labile organic matter (Ventura et al., 2007). In such systems, subsequent abiotic processes of methane formation in the ultramafic rocks have been invoked in the literature such as in the metamorphosed ophicarbonates of the Italian Alps, where Vitale-Brovarone et al. (2017) describe episodic infiltration of highly reducing fluids causing precipitation of graphitic C and mineral-alteration, followed by abiotic methane production through interaction with the graphitic layers (although in this case no $\delta^{13}C$ values are reported). Given the presence of similar mineralogies (carbonate and graphitic layers, ultramafics) in an ancient hydrothermal system such as Kidd Creek, as well as the presence of abundant H_2 typically associated with such water–rock reactions, the identification of abiotic methane in the Kidd Creek fracture waters is at least consistent with a similar process and setting. The specific rates, reactions, and timings surrounding methane production, however, require further investigation.

The remarkably ^{13}C-enriched nature of carbon sources at Kidd Creek extends beyond the organic phases. For the carbonates at Kidd Creek, the range of $\delta^{13}C$ values is, like the TOC $\delta^{13}C$ range (−18 to −33‰; Wellmer et al., 1999), also quite ^{13}C-enriched, with values for carbonates typically between −1 to −5‰. These are again very different from the Precambrian sites where microbial methane has been invoked, where $\delta^{13}C$ values for carbonates trend to as low as −25‰, again correlating with the increasing TOC levels and $\delta^{13}C$ TOC values as ^{13}C-depleted as −48‰ (Wellmer et al., 1999). In fact, all carbon sources at Kidd Creek are quite enriched in ^{13}C. In addition to the solid phases including organic carbon (−18 to −33‰) and carbonates (−1 to −5‰); the dissolved inorganic carbon (DIC) and dissolved organic carbon (DOC) have ranges of $\delta^{13}C$ values of only between −0.5 to −8.8‰; and −5.1 to −8.9‰, respectively (Sherwood Lollar et al., 2021). DIC concentrations are low (typically 30–60 μM). DOC ranges from 2-5 Mm but is remarkably simple in composition – made up almost in entirety of acetate and formate (Sherwood Lollar et al., 2021). The latter provides a good check on the absence of contamination, as surface

fluids used for mine operations have a far more complex DOC load consistent with their origin in a surface lake (Lollar et al., 2019).

Given the variety of potential mechanism to produce abiotic hydrocarbons invoked in the literature, including Sabatier and FTT reactions; surface catalyzed hydrogenation from CO_2 or CO; uncatalyzed aqueous CO_2 reduction, thermal decomposition of carbonates; carbonate-graphite metamorphism (see Etiope and Sherwood Lollar (2013) Table 1 for references), and the paucity, to date, of experiments that explore their full range of compositional and isotopic fractionation patterns, the specific mechanisms of abiotic methane production at Kidd Creek remain unresolved. Any and all of the above are consistent with the geologic, mineralogic and fluid history of the system. While it is not yet clear which of the various carbon sources at Kidd Creek are the ultimate carbon source, it is instructive to note, that the range of the oxidized carbon sources listed above (carbonates, DIC) is about −1 to −8.8‰. Based on the experiments conducted by McCollom et al. (2010) and compiled by McCollom (2013); a carbon source in such a range would be expected to produce abiotic methane that is up to 30–34‰ more depleted. While far from definitive such values are nonetheless within the range of methane observed at Kidd Creek (−32 to −45‰).

1.4. Recent Frameworks for evaluation of biogenicity and abiogenicity

As most recently summarized in Etiope and Sherwood Lollar (2013) and Sherwood Lollar et al. (2008), the interpretational framework for evaluation of potential abiogenic contribution to methane relies on a five-part analysis including:

1. Characterization, to the degree possible, of the entire reaction spectrum of reactants and products involved in the methane cycle (e.g. $\alpha_{DIC\text{-}CH4}$, $\alpha_{H2O\text{-}CH4}$ values, relationships between $\delta^{13}C$ and $\delta^{2}H$ of methane, ethane and higher hydrocarbons)
2. Associated Species (H_2, CO_2, H_2O, noble gases, S species, carbon sources)
3. Geologic and Hydrogeologic Context
4. Evaluation of Potential for Mixing
5. Role of Post-genetic Alteration Processes

This integrated approach is heavily influenced by emerging trends in life detection and biosignatures research (and the corollary – indicators of abiogenicity) arising from the planetary sciences and astrobiology community. Recent work and reports (NASEM, 2018; Hoehler et al. 2020) have emphasized that differentiating biogenicity from abiogenicity, even on Earth, is not a yes/no proposition based on a simple set of criteria. For abiotic methane in particular, the problems with any given proposed criteria or even set of criteria have been critiqued by Sherwood Lollar et al. (2008); Etiope and Sherwood Lollar (2013); and most recently many of the same points from these earlier studies nicely summarized by Reeves and Fiebig (2020) (for summary see Table A1 in the accompanying appendix).

The integrated approach as articulated in the NASEM report *An Astrobiology Strategy for the Search for Life in the Universe* (which we note includes Earth) calls for a "comprehensive framework for assessment of biogenicity - including the potential for abiosignatures, false positives, and false negatives - to guide testing and evaluation of in situ and remote biosignatures." Critically, it states that the evidence for life, or for non-life (abiogenicity) must be evaluated and understood within the context of the environment that hosts it. Practically what this means is rather than a set of criteria (and yes/no propositions), investigation should focus on a set of questions to inform, for any given system, the prevalence and "signal strength" of potential biosignatures, of abiosignatures, and significantly, of any contamination. Context, geochemical baselines, potential primary versus secondary alteration, and spatial and temporal variability in signals, particularly where they may identify mixing effects, are all critical components of such an integrated approach.

Table 1
Mean and standard deviation $\delta^{13}C$, δD, $\Delta^{13}CH_3D$ and $\Delta^{12}CH_2D_2$ for 13 independent analyses of internal standard UCLA-1. All values reported in per mil (‰). The reported standard deviation here is considered to be a reasonable representation of the uncertainty for unknown samples prepared and analysed at UCLA.

Isotopic signal	Mean	1 σ
$\delta^{13}C_{(PDB)}$	−34.97	0.11
$\delta D_{(SMOW)}$	−51.18	0.31
$\Delta^{13}CH_3D$	−0.084	0.22
$\Delta^{12}CH_2D_2$	−1.35	0.58

1.5. Application of an Integrated Framework to Kidd Creek methane investigations

A critical aspect of the contextual evaluation is that not all methane identified at Kidd Creek or at other Precambrian Shield sites we have investigated are abiotic. In most cases there is evidence for methane from different sources. Most commonly a microbially produced methane component is readily identifiable based on multiple observations including for instance $\alpha_{DIC\text{-}CH4}$, $\alpha_{H2O\text{-}CH4}$ values, relationships in the $\delta^{13}C$ and $\delta^{2}H$ of methane, presence or absence of associated gases (e.g. H_2), and confirmatory culture-based and non-culture (genomic) microbial studies. Typical examples include Beatrix Mine in South Africa (Ward et al., 2004); Enonkoski Mine in Finland (Sherwood Lollar et al., 1993a); and Thompson Mine in Canada (Telling et al., 2018). Many subsurface sites in the Precambrian Shield have been shown to be dominated by "textbook" examples of methane produced by microbial CO_2 reduction (Ward et al., 2004; Sherwood Lollar et al., 2006; Lin et al., 2006). At other sites mixing trends identify fracture fluids that range from "textbook" microbial methane, to methane with very different characteristics. For one end-member then, all lines of evidence including compositional, isotopic ($\delta^{13}C$ and $\delta^{2}H$ values for CH_4; $\alpha_{DIC\text{-}CH4}$ and $\alpha_{H2O\text{-}CH4}$ values) as well as culture-based and molecular microbiological evidence are consistent with existing expectations for microbial methanogenesis via CO_2 reduction. Unlike these micro-

bial end-members, the proposed abiogenic gases do not readily fit any of the existing interpretational frameworks for either microbial or thermogenic gas, and do not appear to be controlled by either thermodynamic or enzymatically-mediated isotopic or chemical equilibrium (Sherwood Lollar et al., 2006, 2008).

The presence of these microbial methane end-members, as outlined in Sherwood Lollar et al. (2008) is an important component in the integrated interpretation of the system as it enables, by comparison and contrast, identification of end-members that do not fit into "conventional" microbial methane conceptual models. In fact it is the spatial and temporal variation in these parameters that is a key underpinning of the interpretation that more than one source of methane exists and that the overall variation at most sites is one of mixing to greater or lesser degree. While the possibility exists for a microbial methane with very different attributes than any identified to date (always a potential issue with empirical defined studies and even more so in so-called "extreme" environments) to attribute the observations to such as yet uncharacterized microbial processes would require the environments under investigation to contain **both** conventional "textbook" microbial methane, as well as this previously unrecognized CH_4. Interpreting the entire spectrum of signatures as microbial in origin would require that both "conventional" microbial methane and "unrecognizable" microbial methane exist in the same fracture fluid environments. Hence the 2008 paper continued:

> "*While we do not disagree that microbial processes clearly are capable of producing a wide variation in carbon and hydrogen isotopic fractionation patterns, we are not convinced by this argument alone. Given the lack of fit of these non-microbial end-members to all known microbial and thermogenic interpretational frameworks to date, alternative explanations for the compositional and isotopic features of these gases must be examined. In this light, the contextual information about the Kidd Creek system plays a major role.*"

1.6. Geological and hydrogeological context

Reeves and Fiebig (2020) make steps in the direction of focusing on contextual environment in their insightful comments that point out the important role played by open versus closed systems. They note that many systems traditionally investigated for abiotic methane formation are open systems such as springs or vents where, under open system conditions, organic matter (or microbial communities) may be introduced into the system from nearby sediments, sedimentary rocks or near-surface fluids (through mixing with seawater or recharging groundwaters). In such systems maximum complexity is found and multiple methane sources (microbial, thermogenic and abiotic) may mix, making clear identification of abiotic methane challenging. They highlight the importance of recent work by Klein et al. (2019); Grozeva et al. (2020) and Vitale-Brovarone et al. (2017) all of which demonstrate that the accumulation of abiotic hydrocarbons may be particularly promoted in closed systems. While in open system the contribution of abiotic methane may occur too slowly to outpace thermogenic and microbial contributions, they note: "*Under closed system conditions, inorganic carbon in entrapped hydrothermal fluids may have sufficient time to react with H_2 and form CH_4 and other light hydrocarbon slowly over time*" (Reeves and Fiebig, 2020). Elsewhere they note the kinetic inhibitions on significant abiotic methane formation via magnetite catalysed serpentinization at laboratory timescales, but note that a wider range of potential catalysts (chrome, iron, nickel) and long residence times (they cite decadal) could favour more abiotic methane formation even if at slow rates.

Kidd Creek fracture waters are some of the most "closed" fluid systems that have ever been identified in the continental crust. Time scales of hydrogeologic isolation on the hundreds of millions to more than 2 billion years have been documented (Holland et al., 2013; Warr et al., 2018). Here, as in the deep gold mines of South Africa, the extraordinarily long residence time and closed system fracture fluids mean that even slow rates of H_2 production by radiolysis (estimated at 0.1 to 1 nM/year; Lin et al., 2005a; Sherwood Lollar et al., 2014) can accumulate to readily account for the Mm levels of dissolved H_2 documented in the deep mine fluids (Lin et al., 2005a, 2005b). Mass independent sulfur isotopic signatures in the dissolved SO_4 in the Kidd Creek fluids similarly attest to a hydrogeological closed system in which the sole source of oxidized sulfur is derived from the Archean host rock by indirect radiolytic oxidation processes (Li et al., 2016). Even if rates of H_2 production and associated methane formation by serpentinization are slow in such systems, the presence of disseminated catalysts such as iron, nickel, chromium catalysts in these actively mined host rocks, coupled with immense timescales, define a plausible end-member case for identification of products of abiotic methane processes as products of water–rock reactions accumulate under the type of closed system conditions in fact referenced by Reeves and Fiebig (2020). The evidence at Kidd Creek of Archean Xe isotopic signatures (Holland et al., 2013, Warr et al., 2018), and at Kidd Creek and Mponeng mines, South Africa and the Yilgarn craton Australia, of Precambrian Ne isotopic signatures (Lippmann-Pipke et al., 2011; Kendrick et al., 2011; Holland et al., 2013; Warr et al., 2018) demonstrate long-term *in situ* preservation of noble gas components and suggest these ancient fracture fluids share some characteristics with the trapped fluid inclusions preserved in the same rocks.

This review has emphasized the critical need for an integrated approach that focuses not on a set of individual criteria but on the need for a comprehensive framework of assessment of biogenicity or abiogenicity integrating geologic and hydrogeologic context, geochemical baselines, potential primary versus secondary alteration, and spatial and temporal variability in signals, particularly due to mixing effects. Recent reviews by Etiope and Sherwood Lollar (2013), Schrenk et al. (2013) and Reeves and Fiebig (2020) are in agreement in identifying caveats and potential false negatives/positives for most individual criteria. However that does not mean that technological developments and new observational parameters are not an important aspect

of scientific progress in this challenge. The overall goal of this paper is to evaluate the role of recent progress on clumped methane isotopologues in this difficult challenge of defining biogenicity and abiogenicity, whether than is being done on Earth, or to investigate other planets and moons such as Mars, Enceladus or Titan. Previous work by Young et al. (2017) revealed abiogenic methane (formed via the Sabatier reaction under laboratory conditions) can be extremely depleted in $\Delta^{12}CH_2D_2$ even though $\Delta^{13}CH_3D$ did not show any corresponding depletion. This is particularly noteworthy as depleted $\Delta^{12}CH_2D_2$ values were also observed in a pilot set of natural methane samples from Kidd Creek Mine, from boreholes already considered dominantly abiogenic based on the integrated interpretational framework outlined above (e.g. Sherwood Lollar et al., 1993b, 2006, 2008; Etiope and Sherwood Lollar, 2013). The specific mechanisms surrounding depletion in $\Delta^{12}CH_2D_2$ in abiogenic methane remain an active area of study and are currently attributed to quantum tunnelling effects, combinatorial effects due to δD isotopic differences which arise due to reversibility in one or more steps of abiogenic methanogenesis and or different hydrogen sources (i.e. molecular and water-derived hydrogen), or a combination thereof (Young et al., 2017, Young, 2019, Cao et al., 2019, Taenzer et al., 2020). While Young et al. (2017) addressed only 10 samples, this paper focuses on 31 methane samples from Kidd Creek, of which approximately half were analyzed for both methane isotopologues as well, to evaluate the formation and evolution mechanisms controlling methane in this deep subsurface setting using a combined isotope and isotopologue approach. In addition this new study expands the 2017 pilot dataset to include samples collected over a 9 year period of temporal monitoring of this system, and from two levels of the observatory, providing one of the few isotopologue studies to investigate temporal evolution in methane sources and cycling in the deep subsurface.

2. GEOLOGY OF THE SUPERIOR PROVINCE OF THE CANADIAN SHIELD – KIDD CREEK, TIMMINS, ONTARIO, CANADA

Kidd Creek Observatory is located in an operating mine, situated 24 km from the city of Timmins in Ontario, Canada, within a 2.7 Ga stratiform Volcanogenic Massive Sulphide (VMS) deposit (Thurston et al., 2008). This deposit is part of the Kidd-Munro assemblage which is part of the larger Volcanic Zone section of the Abitibi greenstone belt, a major feature of the Superior Province region of the Canadian Shield (Bleeker and Parrish, 1996). The Kidd Creek deposit comprises a series of steeply dipping interlayered sequence of metasedimentary, ultramafic, mafic, and felsic units. The stringer ore, which is a major economic resource for the region, is principally located within the felsic component and was formed by the circulation of metal and silica rich hydrothermal fluids beneath the sea floor.

The VMS assemblage at Kidd Creek as a whole formed through a series of episodic volcanic eruptions interposed with deposition of argillite to chert carbonaceous sediments during periods of quiescence, all deposited in a shallow seafloor setting at 2.72–2.71 Ga (Thurston et al., 2008). A regional metamorphic event at 2.67–2.69 Ga resulted in entire deposit being metamorphosed to greenschist facies and there was a final, post-depositional, metasomatic event at 2.64 Ga. Since then the area has remained geologically quiescent with estimated temperatures remaining below 100 °C for the past two billion years (Davis et al., 1994; Bleeker and Parrish, 1996; Thurston et al., 2008; Berger et al., 2011; Li et al., 2016).

Kidd Creek Mine was developed as an open pit mine in 1964 to exploit the high copper, zinc and silver content of the VMS deposit. Since then it has expanded at depth to form the deepest base metal mine in North America, presently is operating at a depth of 2.9 km. In this facility the typical mining process utilises a standard exploratory borehole approach. Briefly this entails multiple lateral cores of differing dips taken from boreholes at designated depths to determine the ore content in the surrounding rock. These exploratory boreholes frequently intersect with fluid-filled fractures at pressure within the host rock and, as a result, provide a means for these fracture fluids to drain out (Warr et al., 2018). The fluid volumes involved can be significant and high flow rates (≥1000 mL/min) over significant time periods (several years) have been documented. Gas samples taken from these expelled fluids were analysed for both their elemental and hydrocarbon isotopic compositions as well as their low-abundance methane isotopologues. All gas samples were taken following the methods of Sherwood Lollar et al. (2002) and Ward et al. (2004) which are outlined fully in Section 3.1.

Since the early 1990s, Kidd Creek Mine has served as a key sampling point for scientific investigations for subsurface fluids (Doig et al., 1995; Sherwood Lollar et al., 2002). More recently, a dedicated observatory has been continuously in operation at the 2.4 km level since 2007. Here, the fluid geochemistry has been monitored for over a decade and represent, to our knowledge, the longest temporal study of subsurface fluids available at such a profound depth in the scientific community. Previous studies at this location have focussed on investigating the origin of the dissolved gases (Sherwood Lollar et al., 2002, 2006; Young et al., 2017), deep subsurface habitability (Li et al. 2016, Lollar et al 2019), and fluid residence times uses noble gas analyses (Holland et al. 2013; Warr et al. 2018).

3. SAMPLE COLLECTION AND ANALYSIS

3.1. Sample collection

All samples were collected directly at the borehole collars after the methods outlined in Sherwood Lollar et al. (2002) and Ward et al. (2004) both for this and previous gas-based publications from the Kidd Creek Observatory (Sherwood Lollar et al., 2002; Holland et al., 2013; Young et al., 2017; Warr et al., 2018; Labidi et al., 2020). An inflatable packer was inserted into the borehole opening and inflated to create an air-tight seal to prevent atmospheric contamination. A Tygon tube was connected to the end of the packer which was placed in an inverted,

water-filled, submerged sampling beaker with a Luer attachment at the base. A rubber stopper was used to seal the Luer attachment. Gas samples were then collected through the rubber stopper using a gas-tight syringe with a 22-g syringe needle on which were then injected into pre-evacuated 160 mL borosilicate glass serum vials sealed with air-tight blue butyl rubber stoppers containing 100 μg of saturated $HgCl_2$. These samples were analysed for compositional, conventional isotope, and isotopologue analysis following the methods of previously published studies (e.g. Ward et al., 2004; Onstott et al., 2006; Sherwood Lollar et al., 2006; Young et al., 2017).

3.2. Compositional and conventional isotope analysis

All gas samples were analysed at the Stable Isotope Laboratory at the University of Toronto, after the methods outlined in Ward et al. (2004) and Sherwood Lollar et al. (2006). All compositional analyses were run in triplicate and mean values calculated. Briefly, for hydrocarbon analysis (CH_4, C_2H_6, C_3H_8 and C_4H_{10}) a Varian 3400 Gas Chromatograph (GC) was used in conjunction with a flame ionisation detector (FID). The hydrocarbons were separated by passing each sample through a J&W Scientific GS-Q column (0.32 mm OD × 30 m) using helium as a carrier gas. Initially the column was held at 60 °C for 150 s after which it was increased to 120 °C at a rate of 5 °C/60 s.

To determine the remaining inorganic gas components (H_2, He, O_2, CO_2 and N_2) a Varian 3800 GC was used in conjunction with a micro-thermal conductivity conductor (μTCD) again using the techniques based on Ward et al. (2004) and Sherwood Lollar et al. (2006). Each inorganic compound was separated by passing the sample through a Varian Molecular Sieve 5A PLOT fused silica column (0.53 mm OD × 25 m) using helium for a carrier gas to measure Ar and O_2 and using argon as a carrier gas to measure H_2, He and N_2. For the Ar and O_2 analysis the oven temperature was held at −10 °C to ensure complete separation between Ar and O_2 within the column. For the H_2, He and N_2 analysis the oven temperature was initially set to 10 °C for 600 s after which it was increased to 80 °C at a rate of 25 °C/60 s. For CO_2 an initial temperature of 60 °C with an increase to 250 °C at 20 °C/60 s and a hold time of 360 min was used. In all samples CO_2 was below detection consistent with previous analyses of these highly reducing systems (e.g. Sherwood Lollar et al., 2002; Sherwood Lollar et al., 2006) The ratio of methane to higher hydrocarbons (C_1/C_{2+}) are presented in Table 2.

The $\delta^{13}C$ and δD were measured independently using two different techniques. $\delta^{13}C_{(CH4)}$ and $\delta D_{(CH4)}$ values were measured via continuous flow gas source mass spectrometer at Toronto using a Finnigan MAT 252 ($\delta^{13}C$) and Finnigan MAT Delta$^+$-XL (δD) (Sherwood Lollar et al., 2002) and were independently confirmed during the isotopologue analysis at UCLA (Section 3.3). For the analyses conducted at the Stable Isotope laboratory (Toronto) the technique follows the methods outlined by Sherwood Lollar et al. (2002). As is convention the carbon and hydrogen data are presented in the $\delta^{13}C$ and δD format, which expresses the results (in‰) relative to the IAEA international standards VPDB and VSMOW respectively. Further analytical information regarding isotopic analysis and uncertainty is provided in Sherwood Lollar et al. (2007).

3.3. Isotopologue analysis

Clumped isotopologue analyses of methane in each sample were performed using the high-resolution Panorama Mass Spectrometer at UCLA which also simultaneously measured $\delta^{13}C$ and δD values for these samples. Prior to analysis, gas samples were purified and the methane component isolated using a stainless-steel vacuum line interfaced with a gas chromatograph using the techniques as outlined by Young et al. (2017), Giunta et al. (2019), and Ash et al. (2019). All isotopologue samples were analysed for this study (Young et al., 2017) using the high-resolution Nu Instruments Panorama Mass Spectrometer at UCLA which has the mass resolving power (MRP) to resolve the $^{12}CH_4^+$, $^{13}CH_4^+$, $^{13}CH_3D^+$, $^{12}CH_3D^+$ and $^{12}CH_2D_2^+$ methane ion beams (MRP of ~40,000 or greater - Young et al., 2016). Mass spectrometry was performed using the specific analytical procedures and set up as outlined in previous studies (Young et al., 2017; Ash et al., 2019; Giunta et al., 2019). Summarising briefly, two sets of measurements are made for each methane gas sample, corresponding to two different mass settings for the mass spectrometer. In the first magnet setting (mass setting) the ratios $^{13}CH_4/^{12}CH_4$ and $^{13}CH_3D/^{12}CH_4$ are measured for 20 blocks of 20 pairs of sample-reference gas measurement cycles. In the second mass setting the ratios $^{12}CH_3D/^{12}CH_4$ and $^{12}CH_2D_2/^{12}CH_4$ are measured for 40 blocks of 20 pairs of sample-reference gas measurement cycles. Each measurement cycle of sample or reference gas is a 30 second integration. The numbers of blocks were slightly reduced where the methane concentrations were low to ensure that sufficient gas was available for both mass settings. In order to minimise any pressure effects in the mass spectrometer source, the $^{12}CH_4^+$ ion currents for the reference and sample gases are re-balanced to the same fixed ion current after each measurement cycle. $^{12}CH_4^+$, $^{13}CH_4^+$, and $^{12}CH_3D^+$ ions currents are measured using Faraday cups with 10^{11} Ω resistors. The much lower abundance $^{13}CH_3D^+$ and $^{12}CH_2D_2^+$ ions were counted using an electron multiplier at approximately 10,000 and 200 cps, respectively.

Results for the Toronto isotope ratios are reported in ‰ in the usual delta notation, $\delta^{13}C$ (relative to VPDB) and δD (relative to VSMOW), For the rare, multiply-substituted isotopologue analyses at UCLA, the convention is Δ notation. In this context this symbol represents the ‰ deviation of the abundance of the measured isotopologue ratio from the stochastic ratio calculated from the bulk isotopic composition of the gas using the methods and equations presented in Young et al. (2016, 2017):

$$\Delta^{13}CH_3D = \left[\left(\frac{\left(^{13}CH_3D/\ ^{12}CH_4\right)_{sample}}{\left(^{13}CH_3D/\ ^{12}CH_4\right)_{stochastic}}\right) - 1\right] \times 1000 \quad (1)$$

Table 2
Research Data. $\delta^{13}C$, δD and isotopologue data for samples taken from Kidd Creek Observatory. All values are presented in per mil (‰). Values denoted with[a] represent $\delta^{13}C$ and δD analyses performed by the Stable Isotope Laboratory at the University of Toronto with a corresponding total uncertainty of ±0.5 and ±5‰ respectively (Section 3.4). [b]Denotes values analysed at UCLA with corresponding external $\delta^{13}C$ and δD uncertainties of ±0.11 and ±0.31‰ respectively (See Table 1). Uncertainty for $\Delta^{13}CH_3D$ and $\Delta\ ^{12}CH_2D_2$ were calculated through propagation of measurement errors and are comparable to the external reproducibility stated in Table 1. Samples denoted with * indicate isotopologue values previously published in Young et al. 2017. Also given is the C_1/C_{2+} value representing the ratio of methane to higher hydrocarbons where C_1 represents methane and C_{2+} is the sum of C2 (ethane), C3 (propane), C4 (butane) and C5 (pentane). The uncertainty on each concentration value is ± 5 %. NM denotes data not measured. Days since borehole completion provides time period between drilling completion and the day sampling was done.

Sample	Days since borehole drilled	$\delta^{13}C^a$ (methane)	δD^a (methane)	$\delta^{13}C^a$ (ethane)	δD^a (ethane)	$\delta^{13}C^b$ (methane)	$\delta\ D^b$ (methane)	$\Delta^{13}CH_3D^b$	$\Delta^{12}CH_2D_2^b$	C_1/C_{2+}
Kidd Creek 2.4 km										
11.02.08_KC_7850_BH12299	258	−38.8 ± 0.5	−392 ± 5	−39.9 ± 0.5	−303 ± 5	NM	NM	NM	NM	9.4 ± 0.7
19.06.08_KC_7850_BH12299	387	−38.6 ± 0.5	−388 ± 5	−38.4 ± 0.5	−294 ± 5	NM	NM	NM	NM	9.5 ± 0.7
31.03.09_KC_7850_BH12299	672	−39.8 ± 0.5	−389 ± 5	−38.8 ± 0.5	−289 ± 5	NM	NM	NM	NM	8.6 ± 0.6
12.01.10_KC_7850_BH12299	959	−38.7 ± 0.5	−384 ± 5	−38.3 ± 0.5	−307 ± 5	NM	NM	NM	NM	9.4 ± 0.7
21.10.10_KC_7850_BH12299	1241	−40.4 ± 0.5	−450 ± 5	−40.3 ± 0.5	−303 ± 5	NM	NM	NM	NM	8.6 ± 0.6
01.03.12_KC_7850_BH12299	1738	−40.5 ± 0.5	−388 ± 5	−40.4 ± 0.5	−290 ± 5	NM	NM	NM	NM	9.1 ± 0.6
20.09.13_KC_7850_BH12299	2306	−41.3 ± 0.5	−393 ± 5	−40.6 ± 0.5	−315 ± 5	NM	NM	NM	NM	9.1 ± 0.6
02.04.14_KC_7850_BH12299*	2500	−39.7 ± 0.5	−380 ± 5	−39.8 ± 0.5	−310 ± 5	−39.6 ± 0.1	−391.5 ± 0.3	5.8 ± 0.2	18.0 ± 0.6	8.9 ± 0.6
03.04.14_KC_7850_BH12299	2501	−39.7 ± 0.5	−388 ± 5	−39.9 ± 0.5	−309 ± 5	NM	NM	NM	NM	9.0 ± 0.6
12.07.16_KC_7850_BH12299	3332	−39.1 ± 0.5	−393 ± 5	−39.6 ± 0.5	−301 ± 5	−39.5 ± 0.1	−395.2 ± 0.3	4.3 ± 0.2	16.5 ± 0.8	8.7 ± 0.6
25.01.17_KC_7850_BH12299	3529	−38.5 ± 0.5	NM	−39.8 ± 0.5	NM	−39.4 ± 0.1	−397.3 ± 0.3	4.4 ± 0.2	14.9 ± 0.7	9.3 ± 0.7
06.06.17_KC_7850_BH12299	3661	−39.1 ± 0.5	−393 ± 5	−39.5 ± 0.5	−310 ± 5	−39.4 ± 0.1	−395.5 ± 0.3	3.5 ± 0.2	13.9 ± 0.7	8.8 ± 0.6
10.05.07_KC_7850_BH12261	23	−39.6 ± 0.5	−394 ± 5	−38.5 ± 0.5	−309 ± 5	NM	NM	NM	NM	10.4 ± 0.7
11.02.08_KC_7850_BH12261	300	−40.3 ± 0.5	−391 ± 5	−40.3 ± 0.5	−301 ± 5	NM	NM	NM	NM	10.8 ± 0.8
03.04.14_KC_7850_BH12261	2543	−41.0 ± 0.5	−401 ± 5	−40.6 ± 0.5	−310 ± 5	NM	NM	NM	NM	10.2 ± 0.7
22.10.15_KC_7850_BH12261*	3110	−38.7 ± 0.5	NM	−39.5 ± 0.5	NM	−38.7 ± 0.1	−411.7 ± 0.3	5.8 ± 0.1	16.4 ± 0.7	8.1 ± 0.6
25.01.17_KC_7850_BH12261	3571	−39.6 ± 0.5	NM	−39.4 ± 0.5	NM	−38.5 ± 0.1	−410.3 ± 0.3	4.0 ± 0.2	14.7 ± 0.7	9.0 ± 0.6
06.06.17_KC_7850_BH12261	3703	−38.2 ± 0.5	−406 ± 5	−39.5 ± 0.5	−316 ± 5	−38.5 ± 0.1	−410.5 ± 0.3	3.9 ± 0.1	12.1 ± 0.8	9.3 ± 0.7
27.08.07_KC_7850_BH12287a	119	−40.8 ± 0.5	−383 ± 5	−39.9 ± 0.5	−308 ± 5	NM	NM	NM	NM	9.8 ± 0.7
20.06.08_KC_7850_BH12287a	417	−39.3 ± 0.5	−392 ± 5	−38.8 ± 0.5	−307 ± 5	NM	NM	NM	NM	9.0 ± 0.6
20.09.13_KC_7850_BH12287a*	2335	−42.2 ± 0.5	−393 ± 5	−40.8 ± 0.5	−319 ± 5	−41.4 ± 0.1	−389.5 ± 0.3	5.3 ± 0.2	14.9 ± 0.7	8.7 ± 0.6
02.04.14_KC_7850_BH12287a*	2529	−41.5 ± 0.5	−391 ± 5	−41.4 ± 0.5	−319 ± 5	−41.9 ± 0.1	−391.5 ± 0.3	5.0 ± 0.2	14.0 ± 0.8	8.7 ± 0.6
Kidd Creek 2.9 km										
14.06.12_KC_9500_BH13762*	99	−32.7 ± 0.5	−417 ± 5	−37.2 ± 0.5	−302 ± 5	−32.6 ± 0.1	−422.3 ± 0.3	5.6 ± 0.1	−6.3 ± 0.7	7.4 ± 0.5
16.01.13_KC_9500_BH13762*	315	−34.3 ± 0.5	−420 ± 5	−37.0 ± 0.5	−322 ± 5	−35.9 ± 0.1	−421.3 ± 0.3	6.0 ± 0.1	5.2 ± 0.8	4.9 ± 0.3
01.03.12_KC_9500_BH13684	72	−32.5 ± 0.5	−425 ± 5	−36.5 ± 0.5	−300 ± 5	NM	NM	NM	NM	9.1 ± 0.6
14.06.12_KC_9500_BH13684*	177	−31.9 ± 0.5	−410 ± 5	−37.0 ± 0.5	−297 ± 5	−32.1 ± 0.1	−429.3 ± 0.3	5.8 ± 0.2	−9.9 ± 0.6	7.9 ± 0.6
08.02.12_KC_9500_BH13675	50	−32.0 ± 0.5	NM	−37.0 ± 0.5	NM	NM	NM	NM	NM	5.2 ± 0.4
29.11.12_KC_9500_BH2*	334	−33.3 ± 0.5	−415 ± 5	−37.1 ± 0.5	−310 ± 5	−32.7 ± 0.1	−420.8 ± 0.3	5.2 ± 0.2	−6.3 ± 0.8	6.8 ± 0.5
16.01.13_KC_9500_BH2*	381	−32.9 ± 0.5	−413 ± 5	−36.9 ± 0.5	−292 ± 5	−31.8 ± 0.1	−420.0 ± 0.3	5.3 ± 0.2	−8.5 ± 0.8	6.6 ± 0.5
13.07.16_KC_9500_Bubbling A	N/A	−32.2 ± 0.5	−410 ± 5	−36.5 ± 0.5	−313 ± 5	NM	NM	NM	NM	7.3 ± 0.5
13.07.16_KC_9500_Bubbling B	N/A	−32.6 ± 0.5	−409 ± 5	−36.9 ± 0.5	−313 ± 5	NM	NM	NM	NM	8.3 ± 0.6

$$\Delta^{12}CH_2D_2 = \left[\left(\frac{(\,^{12}CH_2D_2/\,^{12}CH_4)_{sample}}{(\,^{12}CH_2D_2/\,^{12}CH_4)_{stochastic}}\right) - 1\right] \times 1000 \quad (2)$$

The accuracy of these stochastic ratios as derived by the equations of Young et al. (2016, 2017) have recently been independently evaluated by the study by Eldridge et al. (2019) which confirmed agreement within 0.2‰ for $\Delta^{13}CH_3D$ and 0.35‰ for $\Delta^{12}CH_2D_2$.

3.4. Measurement uncertainties

All compositional, carbon isotope ratio, and hydrogen isotope ratio values analysed at the University of Toronto using the analytical technique outlined here have a ±5 %, ±0.5‰ and ±5‰ total uncertainty respectively which incorporates both accuracy and reproducibility after the methods of Sherwood Lollar et al. (2007).

To determine the external reproducibility of samples measured via the Panorama at UCLA an internal laboratory standard (UCLA-1) was independently analysed 13 times. The corresponding mean values and 1 σ error are reported in Table 1 and are representative of the uncertainty for $\delta^{13}C$ and δD values. In the case of $\Delta^{13}CH_3D$ and $\Delta^{12}CH_2D_2$, the external reproducibility indicated by these replicate measurements is consistent, though slightly lower than propagated measurement errors which are derived as per Ash et al. (2019). Accordingly, we consider the propagated errors to be most representative of the total uncertainty for these isotopologues. These propagated errors are provided for each sample in Table 2.

4. RESULTS

4.1. $\delta^{13}C$, δD, and compositional data

The $\delta^{13}C$, δD, compositional and isotopologue data from both laboratories are presented in Table 2. There is good agreement between the $\delta^{13}C$ and δD isotope values measured at the Stable Isotope Laboratory in Toronto and from the Panorama at UCLA (Table 2). Most values lie within reported 1 σ uncertainty of one another and all except two δD values lie within 2 σ. The good agreement between the two data sets (produced via two separate techniques) both reinforces the validity of the values generated via conventional means (GC-IRMS) as well as further highlighting the accuracy of analyses conducted using the Panorama. Given that the data set generated by the Toronto Stable Isotope Laboratory is significantly larger, and covers three separate levels within the observatory (2.4 and 2.9 km data presented here, 2.1 km data taken from Sherwood Lollar et al., 2002), these are the data set which is used to investigate the $\delta^{13}C$ and δD of light hydrocarbons, including methane, at Kidd Creek. These $\delta^{13}C$ and δD data are presented in Fig. 1.

In Fig. 1 the methane isotopic data are plotted in a conventional $\delta^{13}C$-δD plot using the proposed microbial and thermogenic fields from Sherwood Lollar et al. (2006), after Schoell (1988). All Kidd Creek data plot outside of these conventional microbial and thermogenic fields. Samples

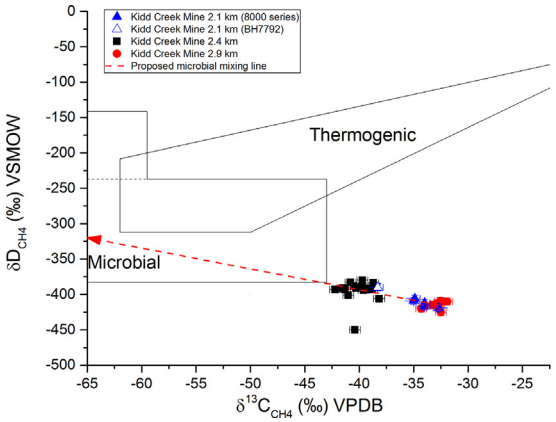

Fig. 1. $\delta^{13}C$ vs δD of methane for samples collected from 2.4 (black squares) and 2.9 km (red circles) below surface. All values presented in per mil (‰). Values for 2.1 km level (open and solid blue triangles) are from Sherwood Lollar et al. (2002, 2008). These previously published samples from 2.1 km are shown in solid blue triangles (8000 series) while the sample collected from borehole 7792 is represented by an open blue triangle. No δD is available for the 6000 series data from 2.1 km and so has not been plotted. A theoretical mixing line indicating the isotopic effect expected from the addition of microbial methane is included (red dashed line). In such a mixing scenario the microbial methane contribution to the most ^{13}C depleted sample from 2.9 km shown here is approximately 22 %. This mixing model uses a hypothetical microbial end-member of −65‰ and −320‰ for $\delta^{13}C$ and δD respectively based on typical microbial methane (e.g. Whiticar, 1999; Etiope et al., 2013). The implications of different possible microbial end-members are described in Section 5.1. (For interpretation of the references to colour in this figure legend, the reader is referred to the web version of this article.)

previously collected from 2.1 km (blue triangles) are also plotted for comparison and these represent the dataset for which abiogenic methane in this locality was first established (Sherwood Lollar et al., 2006). These samples still represent among the most ^{13}C- enriched and most D-depleted values identified at Kidd Creek (8000 series; Table 1 Sherwood Lollar et al., 2002). Borehole 7792 from 2.1 km was an exception to this and based on the offset of this sample towards somewhat more negative $\delta^{13}C$ and more positive δD values (and small changes in $C_1/C2+$ ratio), this and a limited number of other boreholes were to thought to have a small addition of microbial methane (open blue triangle – Fig. 1, taken from Sherwood Lollar et al., 2002). In this study samples collected from 2.9 km show $\delta^{13}C$ and δD isotopic values which overlap with those identified more than 18 years ago at 2.1 km, and share the same characteristics that also support an abiogenic origin for these new gases from the deepest level of Kidd Creek. In contrast, methane gas from the fracture waters at 2.4 km have more ^{13}C depleted values and more D-enriched values relative to gases from 2.9 km and 2.1 km, and instead are closer to those of borehole 7792 from 2.1 km (open blue triangle – Fig. 1). From both Fig. 1 and Table 2 (and Figure B1) no temporal trend is discernible in the $\delta^{13}C$ or δD values as a function of time for any given borehole except for a single borehole at

2.9 km depth (13762) which showed a slight negative shift in $\delta^{13}C$ (–32.7 to −34.3‰) over the 216 days between sampling events. No corresponding shift in δD outside of error was observed, however. The red dashed line represents a theoretical mixing line between the presumably most abiogenic samples (observed at 2.9 and 2.1 km) and a hypothetical microbial end-member of −65‰ and −320‰ for $\delta^{13}C$ and δD respectively. This mixing calculation is fully discussed in Section 5.1.

In Fig. 2 the isotopic data are again plotted in a conventional $\delta^{13}C$ - δD plot using the proposed microbial and thermogenic fields from Sherwood Lollar et al. (2006), after Schoell (1988). Also plotted are the ethane (C_2) $\delta^{13}C$ and δD values for each sample after Sherwood Lollar et al. (2002). Values are additionally plotted for 2.1 km for borehole 7792 and 8000 series from Sherwood Lollar et al. (2002), where published δD values are available. All ethane values are more D-enriched compared to their associated methane. However, samples collected from both 2.9 km and 2.1 km (8000 series – solid blue triangles) show a ^{13}C-enrichment in methane relative to ethane, consistent with the proposed abiogenic polymerisation models of Sherwood Lollar et al. (2008) which also predict depletion in ^{13}C due to preferential polymerisation of ^{12}C-bearing methane (and, at the same time, enrichment in D due to preferential cleaving of ^{1}H-C bonds). In contrast, all methane sampled from 2.4 km, as well as from one 2.1 km borehole (7792 – open blue triangle) have methane values which are more ^{13}C-depleted and are comparable to their associated ethane $\delta^{13}C$ values. Overall these samples from 2.4 km show a relationship between $\delta^{13}C$ of methane and ethane that is significantly different than the abiogenic samples from 2.1 km and 2.9 km – and like borehole 7792, may be explained by addition of a small component of ^{13}C-depleted microbial methane that has little impact on the $\delta^{13}C$ ethane values (likely due to the very small amounts of ethane typically associated with microbial hydrocarbon gases, which have C_1/C_{2+} ratios typically > 1000).

Fig. 3 investigates this potential mixing interpretation further. Here the $\delta^{13}C$ is plotted for methane (C_1) versus the C_1/C_{2+} ratio, where C_{2+} represents higher hydrocarbons (ethane, propane, butane and pentane). In line with Figs. 1 and 2, the proposed microbial field is taken from Sherwood Lollar et al. (2006), modified from Hunt (1996). Both $\delta^{13}C$ values and C_1/C_{2+} ratios for samples collected from 2.4 km are offset compared to the samples from 2.9 km in a direction consistent with a larger contribution of microbial methane to the 2.4 level samples. This new set of data appears to confirm the observation first proposed for the distribution of previously published data for 2.1 km (Sherwood Lollar et al., 2002) where the majority of the 8000 and 6000 series are, like the 2.9 km samples,

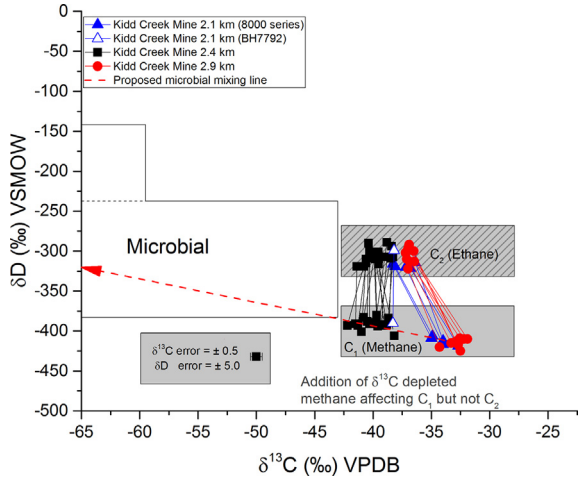

Fig. 2. $\delta^{13}C$ vs δD of methane (C_1) and ethane (C_2) for samples collected from 2.4 and 2.9 km (symbols as in Fig. 1) with published values for 2.1 km from Sherwood Lollar et al. (2002, 2008). All methane and ethane values are highlighted by a solid and patterned box for emphasis. The position of methane relative to ethane has shifted in samples collected from 2.4 km and in one borehole from 2.1 km (BH 7792) relative to samples collected from 2.9 km (this study) and samples from 2.1 km (8000 series - Sherwood Lollar et al., 2002). No δD is available for the 6000 series data from 2.1 km and so has not been plotted. As in Fig. 1, this pattern suggests a dominantly abiogenic end-member for Levels 2.1 and 2.9, and potentially an increasing contribution of microbially produced methane accounting for the more depleted $\delta^{13}C$ value for methane for samples from 2.4 km (and the 7792 sample from 2.1 km). A theoretical mixing line indicating the effect of addition of microbial methane is included (red dashed line) and discussed in Section 5.1.

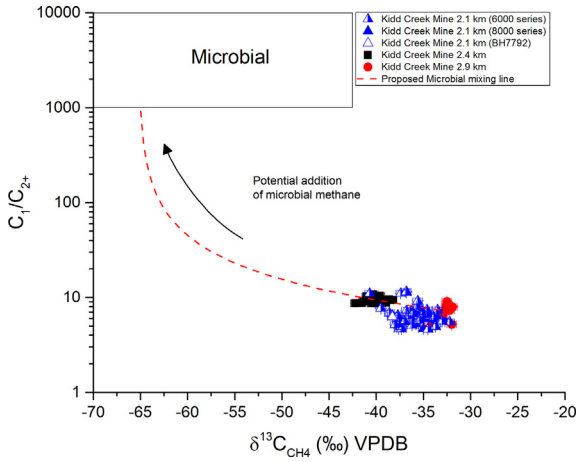

Fig. 3. The $\delta^{13}C$ of methane versus the C_1/C_{2+} ratio based on compositional data (Table 2), where C_1 represents methane and C_{2+} is the sum of C2 (ethane), C_3 (propane), C_4 (butane) and C_5 (pentane). Published values for 2.1 km are from Sherwood Lollar et al. (2002, 2008). Symbols as per legend and Fig. 1. Values for $\delta^{13}C$ are presented in per mil (‰). The potential mixing effect discussed in context of Fig. 2 is further tested here demonstrating that the addition of microbial methane (red dashed line) could account for the small increase in C_1/C_{2+} ratio, and the shift in $\delta^{13}C$ methane values discussed in Section 5.1. In such a mixing scenario the microbial methane contribution to the most 2.9 km $\delta^{13}C$ depleted samples shown here is approximately 23 %. The implications of different possible microbial end-members are described in Section 5.1. (For interpretation of the references to colour in this figure legend, the reader is referred to the web version of this article.)

consistent with a predominantly abiogenic origin, while borehole 7792 from 2.1 km is consistent with an increasing component of microbial methane (Sherwood Lollar et al., 2002). A potential mixing line which incorporates the effect of microbial addition is also included in Fig. 3 as with the previous figures.

4.2. Rare Isotopologue data

As with the $\delta^{13}C$, δD, and compositional data, samples from 2.4 and 2.9 km have different mass-18 isotopologue characteristics as highlighted in Fig. 4. Methane sampled from the deeper level (2.9 km) shows significant deviation from thermodynamic equilibrium, and is strongly depleted in $\Delta^{12}CH_2D_2$ relative to $\Delta^{13}CH_3D$, as is methane formed in abiotic laboratory experiments (Young et al., 2017). By itself the temperature range associated with $\Delta^{13}CH_3D$ values (17–43 °C) appears consistent with the low-temperature geological environment under which the methane is considered to have formed (Sherwood Lollar et al., 2002; Etiope and Sherwood Lollar, 2013; Wang et al., 2015). However, it is not possible to derive a temperature from the negative $\Delta^{12}CH_2D_2$ value due to the marked disequilibrium, and as noted such a lack of concordancy makes the accuracy of temperatures obtained from $\Delta^{13}CH_3D$ alone less reliable. In the one longitudinal study afforded by these data, borehole 13,762 (2.9 km) shows a positive shift in $\Delta^{12}CH_2D_2$ values with time, from a starting value of −6.3 to 5.2 over 216 days (Fig. 4). This represents, to our knowledge, the first data set of field samples to demonstrate temporal evolution on this scale in isotopologue signals. This 11.5‰ positive shift in $\Delta^{12}CH_2D_2$ is associated with the previously mentioned small change in $\delta^{13}C$ (−32.7‰ to −34.3‰), but with no discernible shift in either δD or $\Delta^{13}CH_3D$ outside of error. In contrast, methane sampled from 2.4 km of Kidd Creek indicates $\Delta^{12}CH_2D_2$ and $\Delta^{13}CH_3D$ values closer to the thermodynamic equilibrium line. These data at face value record an apparent temperature ranges of 25–127 °C and 36–91 °C using $\Delta^{13}CH_3D$ and $\Delta^{12}CH_2D_2$ respectively. These temperatures are all above the predicted temperature range at this level (27–33 °C) derived from regional geothermal gradients (Slack 1974; Artemieva and Mooney 2001) and suggest that a degree of disequilibrium is present within samples at this level too, though to a much lesser extent than at 2.9 km. This difference between the two levels principally is on the $\Delta^{12}CH_2D_2$ scale with samples from 2.4 km representing more positive values while $\Delta^{13}CH_3D$ values are relatively consistent between both levels. Similar time evolution was shown by Young et al. (2017), but based on a comparison of time between sampling and opening of various boreholes, rather than specific resampling and monitoring of a single borehole over time. In that study, increases in $\Delta^{12}CH_2D_2$ were associated with positive shifts in δD and negative shifts $\delta^{13}C$ as well.

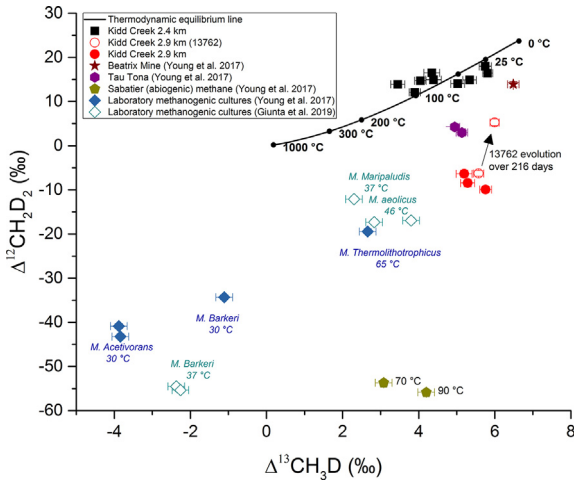

Fig. 4. The low abundance isotopologue data is presented as Δ values, in ‰, relative to the stochastic distribution, after Young et al. (2016). Here $\Delta^{13}CH_3D$ and $\Delta^{12}CH_2D_2$ values of 0 represent the stochastic distribution controlled by thermodynamic equilibrium which is reached at high temperatures (≥727 °C/1000 K). The positively-trending thermodynamic equilibration line (solid black line), calculated by Young et al. (2016), represents the increased association of heavy isotopes with one another as a function of decreasing temperature at equilibrium. Samples from Kidd Creek Level 2.4 km (black squares) and 2.9 km (red circles) are plotted. The temporal variation in data from borehole 13,762 over 216 days is highlighted by the open red circles. Original data taken from Young et al. (2017) as indicated in Table 2. Laboratory culture experiments (blue diamonds, open diamonds), abiogenic methane formed via Sabatier reactions (yellow pentagons) and data from Beatrix Mine (brown star) and Tau Tona (purple hexagon) from Young et al. (2017) and Giunta et al. (2019) are plotted for context (see text). (For interpretation of the references to colour in this figure legend, the reader is referred to the web version of this article.)

5. DISCUSSION

5.1. Evidence for microbial methanogenesis

Both isotopic and microbial lines of evidence have recently demonstrated the presence of microbial activity in the Kidd Creek Mine fracture waters both in the geologic past (Li et al., 2016); and in the present day (Lollar et al., 2019). Specifically, Lollar et al. (2019) successfully confirmed the presence of sulfate reducing bacteria (SRBs) at cell densities of 10^3–10^4 cells/mL in these fluids, activity which had previously been indirectly inferred based on sulfur isotope evidence (Li et al., 2016). For methane, microbially-derived methane is typically identified by a ^{13}C-depleted and D-enriched value relative to abiogenic end-members coupled with a much higher C_1/C_{2+} ratio (e.g. Schoell, 1988; Ward et al., 2004; Sherwood Lollar et al., 2006). The Kidd Creek Observatory provides one of the world's only opportunities to monitor changes in temporal evolution of methane discharges in the deep terrestrial subsurface. As noted, in the previous 2002 study a shift in the isotopic and compositional data, consistent with addition of an estimated 10–25 % microbial methane, was observed over a 19-month period in one of the boreholes at 2.1 km (Sherwood Lollar et al., 2002). As shown in Fig. 3 such a microbial addition can account for $\delta^{13}C$ values for methane which are within error of $\delta^{13}C$ values for

ethane, rather than the 'saw tooth' pattern for C_1-C_4 (methane-butane) which is typically associated with abiogenic methane (e.g. Sherwood Lollar et al., 2002, 2008). As ethane is considered to be principally produced through abiogenic processes at Kidd Creek, this negative $\delta^{13}C$ shift in the position of methane relative to ethane (Fig. 2) was suggested to be indicative of microbial methane addition post-borehole completion (Sherwood Lollar et al., 2002; Sherwood Lollar et al., 2008).

The current study provides novel supporting evidence for an increasing contribution of microbial methane in fracture waters at Kidd Creek post borehole completion. Samples collected at 2.4 km depth are consistent with a microbial component affecting the methane isotopic signal, as suggested in Figs. 1–3 (Schoell, 1988; Sherwood Lollar et al., 1993b, 2006; Ward et al., 2004). Alongside the conventional isotope plots for methane, the $\delta^{13}C$ of methane (−39.9‰) falls within error of ethane (−39.8‰) as shown in Fig. 2. Whereas the 2002 study only identified one borehole that showed such a shift over time, the 2.4 km level data demonstrates a consistent, isotopic offset to values that are more ^{13}C-depleted compared to the more abiogenic end-members at 2.1 and 2.9 km. This is consistent with the hypothesis that the initially abiogenic methane at 2.4 km has incorporated an additional microbial component. Since 2.9 km and 2.1 km continue to preserve a principally abiogenic signal which is geochemically distinct, it follows that fluids sampled at these levels must be hydrogeologically isolated from one another, and that the proposed microbial addition to fluids sampled at 2.4 km occurred post-isolation. This observation is consistent with Warr et al. (2018) who developed a conceptual model proposing hydrogeologic isolation of fracture networks allowing preservation of fluids of different provenances and ages at different depths in deep crustal environments.

As emphasized by recent reviews there is no single diagnostic to decipher methane origin, and so multiple lines of evidence, contextual geological evidence, and the likelihood of mixing, must always be carefully evaluated (Etiope and Sherwood Lollar, 2013 and references therein). It is possible to explore the extent of microbial addition by calculating mixing models using estimates of abiogenic and microbial end-members plausible in these environments. For the purpose of these models the abiogenic end-member was selected by averaging the isotopic value for all samples from 2.9 km. For the microbial end-member, a theoretical $\delta^{13}C$ value of −65‰ was selected (Figs. 1–3) based on typical microbial methane (e.g. Whiticar, 1999; Etiope et al., 2013) and on the typical range identified in previous literature for microbial methane in similar crystalline Shield settings. Whether on the Canadian and Fennoscandian Shields (Sherwood Lollar et al., 1993a; Kietäväinen and Purkamo, 2015 – and references therein; Telling et al., 2018).; South Africa (Ward et al., 2004; Simkus et al., 2016; Lau et al., 2016) the range of $\delta^{13}C$ values for microbial methane is reported between −55 to −65‰ (with C1/C2 + ratios typically between 1000–2000), even where the presence of methanogens has been confirmed by culture-based and non-culture-based genomic investigations (Ward et al, 2004; Lau et al. 2016; Simkus et al., 2016). Only one site in Finland was a reported value more depleted than −65‰ (Kivetty −75.5‰; Kietäväinen and Purkamo, 2015).

Using such a plausible microbial methane $\delta^{13}C$ value (−65‰), such a mixing line indeed passes through the 2.4 km data and defines a corresponding δD value of −320‰ for a theoretical microbial end-member which is also consistent with previously observed methane signatures from other Precambrian rock-hosted environments (e.g. Sherwood Lollar et al., 1993a; 2006; Ward et al., 2004). From this hypothetical mixing line, a 22 % microbial methane addition is theoretically required to generate the 2.4 km isotopic values as highlighted in Fig. 1. Using a more enriched or depleted $\delta^{13}C$ value would increase or decrease this microbial component proportionally. For example other plausible microbial end-member $\delta^{13}C$ values of −70‰ or −55‰ into this model result in a microbial contribution of 19 % and 32% respectively, not substantially different from the estimate of 22%. When the same approach is applied to the C_1/C_{2+} ratios, assuming an abiogenic 2.9 km average of 7.1 and a microbial value of 1000 (to provide a conservative estimate of microbially addition)) a good fit with the data is also observed (Fig. 3). This independent mixing model suggests addition of approximately the same amount of microbial methane (23%) to account for the observed data spread – increasing confidence in this interpretation. This estimate is also in good agreement with previous estimates of 10–25 % microbial methane addition calculated based on borehole 6070 at 2.1 km depth (Sherwood Lollar et al., 2002), suggesting that overall, for this level of the observatory a predominantly abiogenic methane is impacted by a significant, but smaller component of microbially produced methane

There is a clear difference in $\Delta^{13}CH_3D$ and $\Delta^{12}CH_2D_2$ values between samples collected at 2.4 km and at 2.9 km, again consistent with the hydrogeologic isolation of fluids described in the conceptual model of Warr et al. (2018). While samples from 2.9 km show significant $^{12}CH_2D_2$ disequilibrium (Fig. 4), samples collected from 2.4 km appear to consistently plot closer to the equilibrium line. This was previously identified by Young et al. (2017) and attributed to microbial reprocessing through reversibility during methanogenesis and/or bond reordering during microbial AOM. Reversibility by microbial methanogenesis was similarly considered by both Wang et al. (2015) and Stolper et al. (2015) as a potential mechanism for minimising kinetic isotope effects and generating methane close to, or at equilibrium in $\Delta^{13}CH_3D$ space. This 'reversibility' hypothesis was principally considered to occur during the process of microbially-driven methanogenesis and was suggested to be greatest where the availability of substrate (e.g. H_2) was limited and associated production rates were low (Wang et al., 2015; Stolper et al., 2015; Douglas et al., 2016, 2017). The concept of microbial methane potentially forming at thermal equilibrium was initially used as a framework for interpreting natural samples from these and related studies (e.g. Inagaki et al., 2015; Ijiri et al., 2018) where biogenic methane from terrestrial and marine environments yielded apparent $\Delta^{13}CH_3D$ temperatures

consistent with their expected formation conditions. However, the basis of this model is dependent on the reversible nature of methane produced by methanogens; i.e. methanogens must also be able to efficiently oxidise methane (via AOM) at comparable rates to methanogenesis in order to produce and preserve methane at low-temperature equilibrium. A recent review by Timmers et al. (2017) highlighted the following points: 1. Methanogens are only able to perform AOM where net methane production is positive, and 2. methanogens appear to only have a low rate of AOM relative to the methane being produced. This second point draws from three studies all of which independently confirmed that methanogens oxidise relatively minor amounts of methane compared to the total amount of methane being produced (Harder, 1997; Moran et al., 2005, 2007). In other words, the evidence for methanogens to effectively reorder isotopologues of CH_4 to thermodynamic equilibrium distributions is currently lacking or very limited. This is additionally supported by methanogen cultures grown under (laboratory) conditions, which have consistently failed to produce methane close to, or at equilibrium for either $\Delta^{13}CH_3D$ or $\Delta^{12}CH_2D_2$ and instead plot significantly below the equilibrium line in both Δ^{13}CH3D and $\Delta^{12}CH_2D_2$ space (Wang et al., 2015; Stolper et al., 2015; Douglas et al., 2016, 2017, Young et al., 2017; Gruen et al., 2018; Giunta et al., 2019; Young, 2019). Indeed, similar lines of reasoning have been used recently by both Giunta et al. (2019) and Ash et al. (2019) to rule out methanogen-driven re-equilibration in the Antrim Shale and in marine sediments respectively in favour of AOM. Overall, axenic culture experiments suggest that large deviations from equilibrium are the norm for microbial methanogenesis. These observations have been verified in boreal lake environments (Young, 2019). Nevertheless, it is worth noting that these conclusions are based on laboratory cultures with relatively high rates and substrate concentrations, and therefore may not be directly analogous to the low energy environments of the deep subsurface studied here. Consequently, while the experimental evidence favours formation of microbial methane with significant disequilibrium isotopologue signatures, confirmation of the robustness of this conclusion as a function of rates and substrate availability are required before the possibility of 'near-equilibrium' microbial methane production can be ruled out. Nevertheless, based on the current body of evidence from laboratory experiments with methanogenic cultures, it is unlikely that microbial methanogenesis could have produced the more equilibrated, $\Delta^{13}CH_3D$ or $\Delta^{12}CH_2D_2$ values for the samples collected at 2.4 km. Therefore, an additional, subsequent, process must have re-equilibrated the microbial/abiogenic methane mixture at 2.4 km prior to initial sampling. This is discussed in the next section.

5.2. Evidence for methanotrophy

Based on the current evidence from laboratory studies it is unlikely that methanogens produce methane close to, or at, thermodynamic equilibrium, due to associated strong kinetic effects coupled with a low reprocessing ability (Harder, 1997; Moran et al., 2005, 2007; Timmers et al., 2017). Nor can the variation in clumped isotope space between the samples from 2.9 km be due to mixing with potential microbial methane end-members (Fig. 5). In clumped space such abiotic-microbial mixing produces predominantly a horizontal shift to smaller $\Delta^{13}CH_3D$ values and cannot account for the changes in $\Delta^{12}CH_2D_2$ seen within the 2.9 km samples. An additional mechanism is required to account for the temporal variation in 2.9 samples and to have evolved a disequilibrated $\Delta^{13}CH_3D$ and $\Delta^{12}CH_2D_2$ signal over time towards the low-temperature apparent equilibrium values observed in samples from 2.4 km (Fig. 5). One proposed mechanism for re-equilibrating methane isotopologue signatures is microbially-driven anaerobic oxidation of methane (AOM) (Gruen et al., 2018; Ash et al., 2019; Giunta et al., 2019; Young, 2019; Ono et al., 2021). For this form of methanotrophy to be exergonic, methanotrophs require external electron receptors to oxidise methane in the absence of free oxygen. One such acceptor is sulfate (SO_4^{2-}) within anoxic environments. Indeed, many studies have identified the syntrophic nature of methanotrophs and SRBs in anoxic marine sediments and deep crustal systems (e.g. Boetius et al., 2000; Orphan et al., 2001; Elvert et al., 2003; Simkus et al., 2016; Lau et al., 2016). The resultant energy which is released through this metabolic pathway is low, with typical yields between −20 and −40 kJ mol^{-1}, close to the energetic limit for sustaining life (Holler et al., 2011; Timmers et al., 2017 and references therein) and resulting in long biomass doubling times (Nauhaus et al., 2007; Krüger et al., 2008). Such low energy release suggests that the direct substrate-product reaction is close to thermodynamic equilibrium which would therefore typically be associated with a significant degree of reversibility (Holler et al., 2011; Timmers et al., 2017). Indeed, experiments by Holler et al. (2011) into methane formed during enzymatic back reactions during methanotrophy indicate that there could be up to 5.5 % net back flux during AOM. Where substrate availability is limited, such as in low energy deep biosphere environments such as Kidd Creek, the energy release is even smaller, reaction rates are reduced and the enzymatic back-flux can reach as high as 78 % of the net AOM (Yoshinaga et al., 2014; Timmers et al., 2017). The near-equilibrium nature of this reaction coupled with the high likelihood of methane reforming (through reversible reactions) provides a viable mechanism to re-order bonds to a point close to, or at thermodynamic isotopic equilibrium, or to create temporal evolution away from very negative $\Delta^{12}CH_2D_2$ values as the effects of AOM proceed. Indeed, such a mechanism has already been proposed for the Antrim Shale (Giunta et al., 2019) and for marine sediments (Ash et al., 2019) as well as in laboratory experiments (Young, 2019; Ono et al., 2021) and in theoretical/conceptual models of microbial methane cycling (e.g. Wang et al., 2016; Young et al., 2017; Gruen et al., 2018). However, the ability for AOM to promote bond reordering and result in isotopic equilibrium in doubly-substituted isotopologue space, especially in natural settings, requires further investigation and

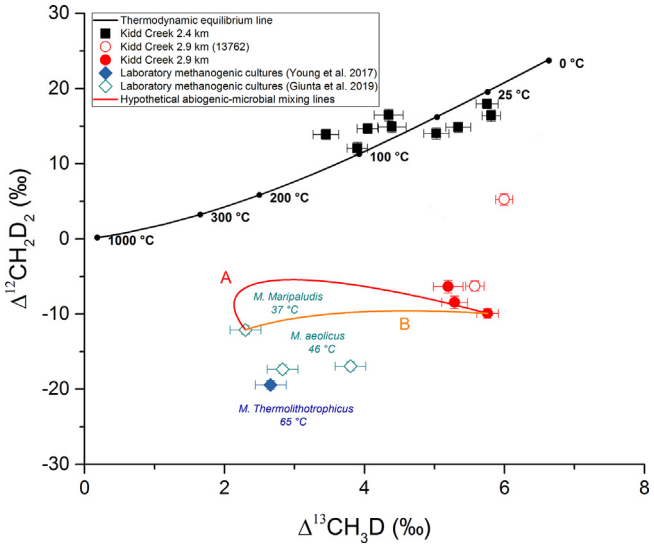

Fig. 5. Demonstrates the effects of mixing between samples collected at 2.9 km (red circles) and possible microbial methane end-members using the calculations of Young et al. (2016; 2017). For both mixing lines the $\Delta^{13}CH_3D$ and $\Delta^{12}CH_2D_2$ values (open diamond) are estimated based on low-temperature (37 °C) hydrogenotrophic laboratory culturing experiments from Giunta et al. (2019). Mixing line A (red) uses a hypothetical microbial end-member based on the values of $\delta^{13}C$ (−65‰) and δD (−320‰) discussed in the main text. Mixing line B (orange) uses the $\Delta^{13}CH_3D$ and $\Delta^{12}CH_2D_2$ values and $\delta^{13}C$ (−50.3‰) and δD (−372.6‰) that correspond to the Giunta et al (2019) hydrogenotrophic laboratory culture. Neither mixing scenario between abiotic and microbial methane can account for the temporal variation at the 2.9 km level (red circles) nor the samples approaching quasi-equilibrium at 2.4 km, and a second process (AOM) is argued to account for that variation (see text). (For interpretation of the references to colour in this figure legend, the reader is referred to the web version of this article.)

remains an active area of current research (e.g. Ono et al., 2021).

With respect to $\delta^{13}C$ and δD, the effect of AOM on the isotopic signatures in most environments is typically associated with isotopic enrichments of the heavy isotopes in the residual methane (e.g. Whiticar, 1999; Seifert et al., 2006; Holler et al., 2009). However, the effects of AOM on the conventional $\delta^{13}C$ and δD values observed for the bulk methane pool are typically small and therefore can be notoriously challenging to identify outside of the laboratory (i.e. within natural systems). This is especially the case where sulfate concentrations are lower than 0.5 mM (Yoshinaga et al. 2014), as they have been shown to be at Kidd Creek (Li et al., 2016). This is further supported by the work of Whiticar (1999) which identified that over 80 % of methane needs to be consumed via AOM before a significant shift in $\delta^{13}C$ can be observed. Any associated isotopic shift in these conventional parameters from AOM is likely minimal, consistent with a high enzymatic back flux in a low energy environment that facilitates high degrees of reprocessing from a relatively low degree of methanotrophy. Similarly, expanding the focus to consider the effects of AOM on dissolved inorganic carbon (DIC) in this case is also equally not straightforward. As the studies of Whiticar et al. (1986) and Whiticar (1999) highlight, the relative carbon isotopic fractionation associated with AOM in natural systems is expected to be much smaller than that from microbial methanogenesis via CO_2 reduction (by potentially an order of magnitude or more). This, combined with the expected low efficiency of AOM in converting methane into DIC under these conditions, would make it difficult, if not impossible to resolve any relatively small isotopic fractionation in the DIC pool arising from AOM where even trace methanogenesis has occurred. Consequently, the $\delta^{13}C_{DIC\text{-}CH4}$ $\delta^{13}C_{DIC\text{-}CH4}$ relationship is not a reliable indicator for identifying the relatively subtle isotope effects of AOM in a most systems, a contributing factor in the historic difficulties in establishing the effects, indeed the presence of AOM, from geochemical signals. Recent papers have highlighted that these long-standing challenges in identifying the effects of AOM in the environment using conventional approaches as one of the particular advantages provided by clumped isotopologue techniques (Gruen et al., 2018; Ash et al., 2019; Giunta et al., 2019; Young, 2019; Thiagarajan et al., 2020b).

To date there is no geochemical or genomic evidence to evaluate the role of anaerobic methanotrophs at Kidd Creek Mine. Such data are available however for several of the other sites shown in Fig. 1. Specifically, methanotrophs (ANMEs) have been positively identified through metagenomic studies at both Beatrix and Tau Tona mines in work by this group in the deep gold mines of South Africa (Simkus et al., 2016; Lau et al., 2016; Magnabosco et al., 2018b). Notably the $\Delta^{13}CH_3D$ and $\Delta^{12}CH_2D_2$ data from these locations (Fig. 4) plot close to the low-temperature equilibrium values observed at 2.4 km of Kidd Creek. Such evidence provides additional contextual support for establishing a link between methanotrophy and bond-reordering in methane isotopologue space. Recent MPN results documenting the presence of SRBs in the fracture fluids at 2.4 km (Lollar et al., 2019) do provide some contextual evidence for the probability of AOM occurring at Kidd Creek as the syntrophic nature of SRBs and methanotrophs is well-documented in both Fennoscandian

and South African Shields subsurface microbial communities (e.g. Bomberg et al., 2015; Simkus et al., 2016; Lau et al., 2016). Based on these lines of evidence, the near-thermodynamic equilibrium $\Delta^{13}CH_3D$ and $\Delta^{12}CH_2D_2$ observed at 2.4 km and over time for borehole 13,762 from 2.9 km may be driven by methanotroph-driven AOM. It is significant that in Figs. 1-3 the bulk conventional parameters are consistent with the samples from 2.4 km being consistent with mixing of up to 22% microbial methane, but the relationship between 2.9 km samples and 2.4 km samples in clumped space does not reflect that mixing. For the 2.4 km samples re-equilibration due to AOM may indeed have gone to quasi-completion. For this low-temperature thermodynamic equilibrium in isotopologue space to be approached, rates of AOM-driven bond-reordering would need to be significantly greater than microbial methanogenesis.

5.3. Temporal constraints

Based on the preceding sections, both abiogenic and microbial methanogenesis, in conjunction with anaerobic microbial methanotrophy have been inferred at Kidd Creek. From the isotopic signatures and temporal changes these processes can be broadly placed in chronological context. These are listed in order below.

1. Abiogenic methane is produced: Consistent with previous studies abiogenic methanogenesis remains the dominant methane type within Kidd Creek Mine (accounting for between 77–100% of the methane pool) throughout all levels. Given the high concentrations of methane (Sherwood Lollar et al., 2002; Sherwood Lollar et al., 2008) and the expected slow abiogenic production rates, especially at the consistent low temperatures anticipated at Kidd Creek (Li et al., 2016 and references therein), this process is expected to have taken place at low rates over significant geological time. Accumulation of significant volumes of abiogenic methane is consistent with the extended (Ga) mean residence times of the fluids identified at this location (Holland et al. 2013; Warr et al. 2018). Due to regional metamorphic activity which lasted until 2.6 Ga (Davis et al., 1994; Bleeker and Parrish, 1996; Li et al., 2016), only methane which formed after this date is expected to have been preserved. This gradual process, driven by water–rock interaction, is likely ongoing and actively producing methane at low rates *in situ* (Sherwood Lollar et al., 2014).

2. Microbial addition of methane: This study has also identified a modest (~22–23 %) microbial methane component present in fluids sampled at 2.4 km based on a microbial end-member mixing model. A microbial component had been previously suggested at 2.1 km in a study by Sherwood Lollar et al. (2002). This addition of microbial methane principally only affected fluids residing at 2.4 km (and the 6000-series subset from 2.1 km) while fracture network fluids at 2.1 and 2.9 km preserve a dominantly abiogenic signal). Accordingly, microbial methane addition can only have occurred after the fracture network(s) sampled at 2.4 km were hydrogeologically isolated from those above and below. This hydrogeologic isolation from at least fluids at 2.9 km was previously confirmed by Warr et al. (2018) using noble gas isotopes.

3. Anaerobic methanotrophy resulting in bond-reordering and re-equilibration of isotopologue signatures: This process accounts for the temporal variation in the time series samples from 2.9 km. It cannot be ruled out that even the most $\Delta^{12}CH_2D_2$ depleted sample from 2.9 km had already been altered by bond-reordering which could account for its position higher than abiotic methane produced in the limited number of Sabatier laboratory experiments to date. Isolated fluids at 2.4 km containing a mixture of abiogenic and microbial methane were also subsequently affected by methanotrophic AOM which 'overprinted' the disequilibrated $\Delta^{13}CH_3D$ and $\Delta^{12}CH_2D_2$ and produced values approaching low temperature equilibrium. This step suggests that AOM-driven bond reordering was the dominant process affecting methane (i.e. methanotrophy occurring at a significantly greater rate than microbial methanogenesis).

4. A final set of observations suggests the effects of ongoing low-level microbial activity. Fig. 6A and B show, since the onset of sampling, trends in mass-18 isotopologue space as all three boreholes at 2.4 km show a shift to smaller $\Delta^{13}CH_3D$ and $\Delta^{12}CH_2D_2$ values over time. To test whether these post-sampling shifts could be due to increased activity of methanogens in the boreholes fluids a mixing model was developed (Figure B2) using both the microbial methane from the laboratory culture of Giunta et al. (2019) discussed earlier, as well as additional microbial methane cultures published by Gruen et al. (2018). Either microbial methane end-member mixing with the 2.4 km methane as originally sampled, could account for the shifts in $\Delta^{13}CH_3D$ and $\Delta^{12}CH_2D_2$ values over time. Despite these changes in isotopologue space, the bulk $\delta^{13}C$ and δD values show no trends within uncertainty (Figure B1). The data suggest the more sensitive isotopologues are providing information about on-going processes in the boreholes post-sampling. Determination of the abundance and nature of the subsurface anaerobic microbial communities, and their effect on the geochemistry, are in the process of being investigated by research teams globally, focussing on the Canadian Shield (Li et al., 2016; Telling et al., 2018; Lollar et al., 2019), the South African Craton (Lin et al., 2006; Magnabosco et al., 2016; Lau et al., 2016) and the Fennoscandian Shield (Pedersen, 2012; Purkamo et al., 2016; Kietäväinen et al., 2017). From these, and ongoing genomic studies it is expected that rates and mechanisms of microbial methanogenesis and ANME-driven AOM will be better constrained and add additional constraints on this matter.

6. CONCLUSIONS AND FUTURE WORK

Through a combined compositional, isotopic, and isotopologue approach this study provides evidence for microbiological activity including microbial methanogenesis and anaerobic methane oxidation in the fracture fluids and associated dissolved gases Kidd Creek Observatory more than 2 km below surface (Sherwood Lollar et al., 2002; Li et al., 2016; Young et al., 2017; Lollar et al., 2019). The

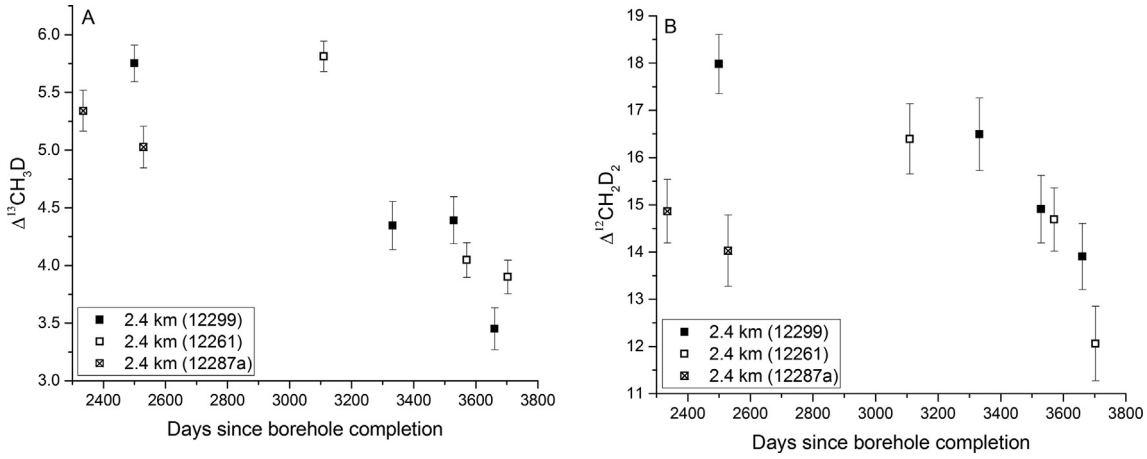

Fig. 6. (A and B) The $\Delta^{13}CH_3D$ (A) and $\Delta^{12}CH_2D_2$ (B) isotopologue signal for the three boreholes at 2.4 km sampled as a function of time after initial sampling. Both isotopologues indicate a recent shift outside of error during the monitoring period which suggests an increase in microbially derived methane within the fluids has occurred during sampling at this level. See Appendix B for additional discussion.

genomic and metagenomic details of microbial organisms and communities here have yet to be fully characterised but the identification of relevant processes via the geochemical and isotopic techniques in this study provide insights into the relative rates and timings of microbiological processes occurring at Kidd Creek and on the relative contributions of abiotic and microbial processes to the deep methane cycle at the site. The findings have broad implications for our understanding of the deep subsurface biosphere, the diversity of microbial organisms in the subsurface and the relative contributions of abiotic organic synthesis and biological sources of methane in a deep Earth analog environment relevant to the discoveries of methane in the Mars atmosphere recently confirmed by the Curiosity Rover.

Declaration of Competing Interest

The authors declare that they have no known competing financial interests or personal relationships that could have appeared to influence the work reported in this paper.

ACKNOWLEDGEMENTS

This study was financially supported by the Canada Research Chairs program, Natural Sciences and Engineering Research Council of Canada Discovery and Accelerator grants, and additional funding provided by the Deep Carbon Observatory, CIFAR and the Nuclear Waste Management Organisation (NWMO). The senior author on this study (Sherwood Lollar) is a Fellow of the CIFAR Earth 4D Subsurface Science and Exploration program. Thanks are due to colleagues and supporters at the mines whose efforts and support for the sampling program were invaluable.

APPENDIX A. SUPPLEMENTARY MATERIAL

Supplementary data to this article can be found online at https://doi.org/10.1016/j.gca.2020.12.002.

REFERENCES

Artemieva I. M. and Mooney W. D. (2001) Thermal thickness and evolution of Precambrian lithosphere: A global study. *J. Geophys. Res.* **106**, 16387–16414.

Ash J. L., Egger M., Treude T., Kohl I., Cragg B., Parkes R. J., Slomp C. P., Sherwood Lollar B. and Young E. D. (2019) Exchange catalysis during anaerobic methanotrophy revealed by $^{12}CH_2D_2$ and $^{13}CH_3D$ in methane. *Geochemical Perspect. Lett.* **10**, 26–30.

Berger B. R., Bleeker W., van Breemen O., Chapman J. B., Peter J. M., Layton-Matthews D. and Gemmell J. B. (2011) Results from the Targeted Geoscience Initiative III Kidd-Munro Project. *Open File Rep.* **6258**.

Bleeker W. and Parrish R. R. (1996) Stratigraphy and U-Pb zircon geochronology of Kidd Creek: Implications for the formation of giant volcanogenic massive sulphide deposits and the tectonic history of the Abitibi greenstone belt. *Can. J. Earth Sci.* **33**, 1213–1231.

Boetius A., Ravenschlag K., Schubert C. J., Rickert D., Widdel F., Gieseke A., Amann R., Jørgensen B. B., Witte U. and Pfannkuche O. (2000) A marine microbial consortium apparently mediating anaerobic oxidation of methane. *Nature* **407**, 623–626.

Bomberg M., Nyyssönen M., Pitkänen P., Lehtinen A. and Itävaara M. (2015) Active microbial communities inhabit sulphate-methane interphase in deep bedrock fracture fluids in Olkiluoto, Finland. Biomed Res. Int. 2015.

Cao X., Bao H. and Peng Y. (2019) A kinetic model for isotopologue signatures of methane generated by biotic and abiotic CO_2 methanation. *Geochim. Cosmochim. Acta* **249**, 59–75.

Clark I. D. and Fritz P. (1997) Environmental isotopes in hydrogeology. CRC press. 328 pp.

Davis D. W., Schandl E. S. and Wasteneys H. A. (1994) U-Pb dating of minerals in alteration halos of Superior Province massive sulfide deposits: syngenesis versus metamorphism. *Contrib. to Mineral. Petrol.* **115**, 427–437.

Doig F., Sherwood Lollar B. and Ferris F. G. (1995) Evidence for abundant microbial communities in Canadian Shield groundwaters – an in situ biofilm experiment. *Geomicrobiol. J.* **13**, 91–101.

Douglas P. M. J., Stolper D. A., Eiler J. M., Sessions A. L., Lawson M., Shuai Y., Bishop A., Podlaha O. G., Ferreira A.

A., Santos Neto E. V., Niemann M., Steen A. S., Huang L., Chimiak L., Valentine D. L., Fiebig J., Luhmann A. J., Seyfried W. E., Etiope G., Schoell M., Inskeep W. P., Moran J. J. and Kitchen N. (2017) Methane clumped isotopes: Progress and potential for a new isotopic tracer. *Org. Geochem.* **113**, 262–282.

Douglas P. M. J., Stolper D. A., Smith D. A., Walter Anthony K. M., Paull C. K., Dallimore S., Wik M., Crill P. M., Winterdahl M., Eiler J. M. and Sessions A. L. (2016) Diverse origins of Arctic and Subarctic methane point source emissions identified with multiply-substituted isotopologues. *Geochim. Cosmochim. Acta* **188**, 163–188.

Drake H., Heim C., Roberts N. M. W., Zack T., Tillberg M., Broman C., Ivarsson M., Whitehouse M. J. and Åström M. E. (2017) Isotopic evidence for microbial production and consumption of methane in the upper continental crust throughout the Phanerozoic eon. *Earth Planet. Sci. Lett.* **470**, 108–118.

Eiler J. M. (2007) "Clumped-isotope" geochemistry—The study of naturally-occurring, multiply-substituted isotopologues. *Earth Planet. Sci. Lett.* **262**, 309–327.

Eldridge D. L., Korol R., Lloyd M. K., Turner A. C., Webb M. A., Miller T. F. and Stolper D. (2019) Comparison of Experimental vs. Theoretical Abundances of $^{13}CH_3D$ and $^{12}CH_2D_2$ for Isotopically Equilibrated Systems From 1–500°C. *ACS Earth Sp. Chem.* **3**, 2747–2764.

Elvert M., Boetius A., Knittel K. and Jørgensen B. B. (2003) Characterization of Specific Membrane Fatty Acids as Chemotaxonomic Markers for Sulfate-Reducing Bacteria Involved in Anaerobic Oxidation of Methane. *Geomicrobiol. J.* **20**, 403–419.

Etiope G., Ehlmann B. L. and Schoell M. (2013) Low temperature production and exhalation of methane from serpentinized rocks on Earth: A potential analog for methane production on Mars. *Icarus* **224**, 276–285.

Etiope G. and Sherwood Lollar B. (2013) Abiotic methane on Earth. *Rev. Geophys.* **51**, 276–299.

Giunta T., Young E. D., Warr O., Kohl I., Ash J. L., Martini A., Mundle S. O. C., Rumble D., Pérez-Rodríguez I., Wasley M., LaRowe D. E., Gilbert A. and Sherwood Lollar B. (2019) Methane sources and sinks in continental sedimentary systems: New insights from paired clumped isotopologues $^{13}CH_3D$ and $^{12}CH_2D_2$. *Geochim. Cosmochim. Acta* **245**, 327–351.

Gleeson T., Befus K. M., Jasechko S., Luijendijk E. and Cardenas M. B. (2016) The global volume and distribution of modern groundwater. *Nat. Geosci.* **9**, 161–167.

Grozeva N. G., Klein F., Seewald J. S. and Sylva S. P. (2020) Chemical and isotopic analyses of hydrocarbon-bearing fluid inclusions in olivine-rich rocks. *Philos. Trans. R. Soc. A* **378**, 20190332.

Goodwin A. M. (1996) Chapter 1 - Distribution and Tectonic Setting of Precambrian Crust. In Principles of Precambrian Geology Academic Press, London. pp. 1–50.

Gropp J., Iron M. A. and Halevy I. (2020) Theoretical estimates of equilibrium carbon and hydrogen isotope effects in microbial methane production and anaerobic oxidation of methane. Geochim. Cosmochim. Acta (in press) https://doi.org/10.1016/j.gca.2020.10.018.

Gruen D. S., Wang D. T., Könneke M., Topçuoğlu B. D., Stewart L. C., Goldhammer T., Holden J. F., Hinrichs K. U. and Ono S. (2018) Experimental investigation on the controls of clumped isotopologue and hydrogen isotope ratios in microbial methane. *Geochim. Cosmochim. Acta* **237**, 339–356.

Harder J. (1997) Anaerobic methane oxidation by bacteria employing ^{14}C-methane uncontaminated with ^{14}C-carbon monoxide. *Marine Geol.* **1–2**, 13–23.

Hoehler T., Bains W., Davila A., Parenteau M. and Pohorille A. (2020). Life's requirements, habitability, and biological potential. In Planetary Astrobiology (eds. V. Meadows, D. J. Des Marais, G. Arney, and B. Schmidt). University of Arizona Press: Tucson, AZ, USA.

Holland G., Sherwood Lollar B., Li L., Lacrampe-Couloume G., Slater G. F. and Ballentine C. J. (2013) Deep fracture fluids isolated in the crust since the Precambrian era. *Nature* **497**, 357–360.

Holler T., Wegener G., Knittel K., Boetius A., Brunner B., Kuypers M. M. M. and Widdel F. (2009) Substantial $^{13}C/^{12}C$ and D/H fractionation during anaerobic oxidation of methane by marine consortia enriched *in vitro*. *Environ. Microbiol. Rep.* **1**, 370–376.

Holler T., Wegener G., Niemann H., Deusner C., Ferdelman T. G., Boetius A., Brunner B. and Widdel F. (2011) Carbon and sulfur back flux during anaerobic microbial oxidation of methane and coupled sulfate reduction. *Proc. Natl. Acad. Sci.* **108**, E1484–E1490.

Hunt J. (1996) Petroleum Geochemistry and Geology. Vol. 2, 1–743.

Ijiri A., Inagaki F., Kubo Y., Adhikari R. R., Hattori S., Hoshino T., Imachi H., Kawagucci S., Morono Y., Ohtomo Y., Ono S., Sakai S., Takai K., Toki T., Wang D. T., Yoshinaga M. Y., Arnold G. L., Ashi J., Case D. H., Feseker T., Hinrichs K. U., Ikegawa Y., Ikehara M., Kallmeyer J., Kumagai H., Lever M. A., Morita S., Nakamura K., Nakamura Y., Nishizawa M., Orphan V. J., Røy H., Schmidt F., Tani A., Tanikawa W., Terada T., Tomaru H., Tsuji T., Tsunogai U., Yamaguchi Y. T. and Yoshida N. (2018) Deep-biosphere methane production stimulated by geofluids in the nankai accretionary complex. *Sci. Adv.* **4**(6).

Inagaki F., Kubo Y., Bowles M. W., Heuer V. B., Ijiri A., Imachi H., Ito M., Kaneko M., Lever M. A., Morita S., Morono Y., Tanikawa W., Bihan M., Bowden S. A., Elvert M., Glombitza C., Gross D., Harrington G. J., Hori T., Li K., Limmer D., Murayama M., Ohkouchi N., Ono S., Purkey M., Sanada Y., Sauvage J., Snyder G., Takano Y., Tasumi E., Terada T., Tomaru H., Wang D. T. and Yamada Y. (2015) Exploring deep microbial life in coal-bearing sediment down to ~2.5 km below the ocean floor. *Science* **349**, 420–424.

Kendrick M. A., Honda M., Walshe J. and Petersen K. (2011) Fluid sources and the role of abiogenic-CH_4 in Archean gold mineralization: Constraints from noble gases and halogens. *Precambrian Res.* **189**, 313–327.

Kietäväinen R., Ahonen L., Niinikoski P., Nykänen H. and Kukkonen I. T. (2017) Abiotic and biotic controls on methane formation down to 2.5 km depth within the Precambrian Fennoscandian Shield. *Geochim. Cosmochim. Acta* **202**, 124–145.

Kietäväinen R. and Purkamo L. (2015) The origin, source, and cycling of methane in deep crystalline rock biosphere. *Front. Microbiol.* **6**, 725.

Klein F., Grozeva N. G. and Seewald J. S. (2019) Abiotic methane synthesis and serpentinization in olivine-hosted fluid inclusions. *Proc. Natl. Acad. Sci.* **116**, 17666–17672.

Krüger M., Wolters H., Gehre M., Joye S. B. and Richnow H. H. (2008) Tracing the slow growth of anaerobic methane-oxidizing communities by ^{15}N-labelling techniques. *FEMS Microbiol. Ecol.* **63**, 401–411.

Labidi J., Barry P. H., Bekaert D. V., Broadley M. W., Marty B., Giunta T., Warr O., Sherwood Lollar B., Fischer T. P., Avice G., Caracausi A., Ballentine C. J., Halldórsson S. A., Stefánsson A., Kurz M. D., Kohl I. E. and Young E. D. (2020) Hydrothermal 15N15N abundances constrain the origins of mantle nitrogen. *Nature* **580**, 367–371.

Lau M. C. Y., Kieft T. L., Kuloyo O., Linage-Alvarez B., van Heerden E., Lindsay M. R., Magnabosco C., Wang W.,

Wiggins R. L., Guo L., Perlman D. H., Kyin S., Shwe H. H., Harris R. L., Oh Y., Yi M. J., Purtschert R., Slater G. F., Ono S., Wei S., Li L., Sherwood Lollar B. and Onstott T. C. (2016) An oligotrophic deep-subsurface community dependent on syntrophy is dominated by sulfur-driven autotrophic denitrifiers. *Proc. Natl. Acad. Sci.* **113**, E7927–E7936.

Li L., Wing B. A., Bui T. H., McDermott J. M., Slater G. F., Wei S., Lacrampe-Couloume G. and Sherwood Lollar B. (2016) Sulfur mass-independent fractionation in subsurface fracture waters indicates a long-standing sulfur cycle in Precambrian rocks. *Nat. Commun.* **7**, 13252.

Lin L. H., Hall J., Lippmann-Pipke J., Ward J. A., Sherwood Lollar B., DeFlaun M., Rothmel R., Moser D., Gihring T. M., Mislowack B. and Onstott T. C. (2005a) Radiolytic H_2 in continental crust: Nuclear power for deep subsurface microbial communities. *Geochemistry, Geophys. Geosystems* **6**, 13 pp.

Lin L. H., Slater G. F., Sherwood Lollar B., Lacrampe-Couloume G. and Onstott T. C. (2005b) The yield and isotopic composition of radiolytic H_2, a potential energy source for the deep subsurface biosphere. *Geochim. Cosmochim. Acta* **69**, 893–903.

Lin L. H., Wang P. L., Rumble D., Lippmann-Pipke J., Boice E., Pratt L. M., Sherwood Lollar B., Brodie E. L., Hazen T. C., Andersen G. L., DeSantis T. Z., Moser D. P., Kershaw D. and Onstott T. C. (2006) Long-term sustainability of a high-energy, low-diversity crustal biome. *Science* **314**, 479–482.

Lippmann-Pipke J., Sherwood Lollar B., Niedermann S., Stroncik N. A., Naumann R., van Heerden E. and Onstott T. C. (2011) Neon identifies two billion year old fluid component in Kaapvaal Craton. *Chem. Geol.* **283**, 287–296.

Lollar G. S., Warr O., Telling J., Osburn M. R. and Sherwood Lollar B. (2019) 'Follow the Water': Hydrogeochemical Constraints on Microbial Investigations 2.4 km Below Surface at the Kidd Creek Deep Fluid and Deep Life Observatory. *Geomicrobiol. J.* **1–14**.

Ma Q., Wu S. and Tang Y. (2008) Formation and abundance of doubly-substituted methane isotopologues (13CH3D) in natural gas systems. *Geochim. Cosmochim. Acta* **72**, 5446–5456.

Magnabosco C., Ryan K., Lau M. C. Y., Kuloyo O., Sherwood Lollar B., Kieft T. L., van Heerden E. and Onstott T. C. (2016) A metagenomic window into carbon metabolism at 3 km depth in Precambrian continental crust. *ISME J.* **10**, 730–741.

Magnabosco C., Lin L.-H., Dong H., Bomberg M., Ghiorse W., Stan-Lotter H., Perdersen K., Kieft T. L., van Heerden E. and Onstott T. C. (2018a) The biomass and biodiversity of the continental subsurface. *Nat. Geosci.* **11**, 707–717.

Magnabosco C., Timmers P. H. A., Lau M. C. Y., Borgonie G., Linage-Alvarez B., Kuloyo O., Alleva R., Kieft T. L., Slater G. F., van Heerden E., Sherwood Lollar B. and Onstott T. C. (2018b) Fluctuations in populations of subsurface methane oxidizers in coordination with changes in electron acceptor availability. *FEMS Microbiol. Ecol.* **97**(7).

McCollom T. M. (2013) Laboratory simulations of abiotic hydrocarbon formation in Earth's deep subsurface. *Rev. Mineral. Geochemistry* **75**, 467–494.

McCollom T. M., Sherwood Lollar B., Lacrampe-Couloume G. and Seewald J. S. (2010) The influence of carbon source on abiotic organic synthesis and carbon isotope fractionation under hydrothermal conditions. *Geochim. Cosmochim. Acta* **74**, 2717–2740.

Moran J. J., House C. H., Freeman K. H. and Ferry J. G. (2005) Trace methane oxidation studied in several Euryarchaeota under diverse conditions. *Archaea* **1**, 303–309.

Moran J. J., House C. H., Thomas B. and Freeman K. H. (2007) Products of trace methane oxidation during nonmethyltrophic growth by Methanosarcina. *J. Geophys. Res. Biogeosciences* **112**, G2.

Nauhaus K., Albrecht M., Elvert M., Boetius A. and Widdel F. (2007) In vitro cell growth of marine archaeal-bacterial consortia during anaerobic oxidation of methane with sulfate. *Environ. Microbiol.* **9**, 187–196.

NASEM (National Academies of Sciences, Engineering, and Medicine) (2018) An Astrobiology Science Strategy for the Search for Life in the Universe. The National Academies Press.

Ono S., Rhim J. H., Gruen D. S., Taubner H., Kölling M. and Wegener G. (2021) Clumped isotopologue fractionation by microbial cultures performing the anaerobic oxidation of methane. *Geochim. Cosmochim. Acta* **293**, 70–85.

Ono S., Wang D. T., Gruen D. S., Sherwood Lollar B., Zahniser M. S., McManus B. J. and Nelson D. D. (2014) Measurement of a Doubly Substituted Methane Isotopologue, $^{13}CH_3D$, by Tunable Infrared Laser Direct Absorption Spectroscopy. *Anal. Chem.* **86**, 6487–6494.

Onstott T. C., Lin L.-H., Davidson M., Mislowack B., Borcsik M., Hall J., Slater G., Ward J., Sherwood Lollar B., Lippmann-Pipke J., Boice E., Pratt L. M., Pfiffner S., Moser D., Gihring T., Kieft T. L., Phelps T. J., Vanheerden E., Litthaur D., Deflaun M., Rothmel R., Wanger G. and Southam G. (2006) The Origin and Age of Biogeochemical Trends in Deep Fracture Water of the Witwatersrand Basin, South Africa. *Geomicrobiol. J.* **23**, 369–414.

Orphan V. J., Hinrichs K. U., Ussler W., Paull C. K., Taylor L. T., Sylva S. P., Hayes J. M. and Delong E. F. (2001) Comparative Analysis of Methane-Oxidizing Archaea and Sulfate-Reducing Bacteria in Anoxic Marine Sediments. *Appl. Environ. Microbiol.* **67**, 1922–1934.

Parnell J. and Blamey N. (2017) Global hydrogen reservoirs in basement and basins. *Geochem. Trans* **18**, 2.

Pedersen K. (2012) Influence of H_2 and O_2 on sulphate-reducing activity of a subterranean community and the coupled response in redox potential. *FEMS Microbiol. Ecol.* **82**, 653–665.

Purkamo L., Bomberg M., Kietäväinen R., Salavirta H., Nyyssönen M., Nuppunen-Puputti M., Ahonen L., Kukkonen I. and Itävaara M. (2016) Microbial co-occurrence patterns in deep Precambrian bedrock fracture fluids. *Biogeosciences* **13**, 3091–3108.

Reeves E. P. and Fiebig J. (2020) Abiotic synthesis of methane and organic compounds in Earth's lithosphere. *Elements* **16**, 25–31.

Schoell M. (1988) Multiple origins of methane in the Earth. *Chem. Geol.* **71**, 1–10.

Schrenk M. O., Brazelton W. J. and Lang S. (2013). Serpentinization, carbon, and deep life. In Carbon in Earth. Rev. Mineral. Geochem (R.M. Hazen, Jones A. P and Baross, J A. (Eds.)). 75, 576–606.

Seifert R., Nauhaus K., Blumenberg M., Krüger M. and Michaelis W. (2006) Methane dynamics in a microbial community of the Black Sea traced by stable carbon isotopes in vitro. *Org. Geochem.* **37**, 1411–1419.

Sherwood Lollar B., Frape S. K., Fritz P., Macko S. A., Welhan J. A., Blomqvist R. and Lahermo P. W. (1993a) Evidence for bacterially generated hydrocarbon gas in Canadian shield and fennoscandian shield rocks. *Geochim. Cosmochim. Acta* **57**, 5073–5085.

Sherwood Lollar B., Frape S. K., Weise S. M., Fritz P., Macko S. A. and Welhan J. A. (1993b) Abiogenic methanogenesis in crystalline rocks. *Geochim. Cosmochim. Acta* **57**, 5087–5097.

Sherwood Lollar B., Heur V. B., McDermott J. M., Tille S., Warr O., Moran J. J., Telling J. and Hinrichs K.-U. (2021). AWindow into the Abiotic Carbon Cycle - Volatile Fatty Acids in fracture waters in 2.7 billion year-old host rocks of the Canadian Shield. *Geochim. Cosmochim. Acta* **294**, 295–314. https://doi.org/10.1016/j.gca.2020.11.026.

Sherwood Lollar B., Hirschorn S. K., Chartrand M. M. G. and Lacrampe-Couloume G. (2007) An approach for assessing total instrumental uncertainty in compound-specific carbon isotope analysis: Implications for environmental remediation studies. *Anal. Chem.* **79**, 3469–3475.

Sherwood Lollar B., Lacrampe-Couloume G., Slater G. F., Ward J., Moser D. P., Gihring T. M., Lin L. H. and Onstott T. C. (2006) Unravelling abiogenic and biogenic sources of methane in the Earth's deep subsurface. *Chem. Geol.* **226**, 328–339.

Sherwood Lollar B., Lacrampe-Couloume G., Voglesonger K., Onstott T. C., Pratt L. M. and Slater G. F. (2008) Isotopic signatures of CH_4 and higher hydrocarbon gases from Precambrian Shield sites: A model for abiogenic polymerization of hydrocarbons. *Geochim. Cosmochim. Acta* **72**, 4778–4795.

Sherwood Lollar B., Onstott T. C., Lacrampe-Couloume G. and Ballentine C. J. (2014) The contribution of the Precambrian continental lithosphere to global H_2 production. *Nature* **516**, 379–382.

Sherwood Lollar B., Westgate T. D., Ward J. A., Slater G. F. and Lacrampe-Couloume G. (2002) Abiogenic formation of alkanes in the Earth's crust as a minor source for global hydrocarbon reservoirs. *Nature* **416**, 522–524.

Schoell M. and Wellmer F.-W. (1981) Anomalous 13C depletion in early Precambrian graphites from Superior Province, Canada. *Nature* **290**, 696–699.

Shuai Y., Douglas P. M. J., Zhang S., Stolper D. A., Ellis G. S., Lawson M., Lewan M. D., Formolo M., Mi J., He K., Hu G. and Eiler J. M. (2018) Equilibrium and non-equilibrium controls on the abundances of clumped isotopologues of methane during thermogenic formation in laboratory experiments: Implications for the chemistry of pyrolysis and the origins of natural gases. *Geochim. Cosmochim. Acta* **223**, 159–174.

Simkus D. N., Slater G. F., Sherwood Lollar B., Wilkie K., Kieft T. L., Magnabosco C., Lau M. C. Y., Pullin M. J., Hendrickson S. B., Wommack K. E., Sakowski E. G., van Heerden E., Kuloyo O., Linage B., Borgonie G. and Onstott T. C. (2016) Variations in microbial carbon sources and cycling in the deep continental subsurface. *Geochim. Cosmochim. Acta* **173**, 264–283.

Slack P. (1974) Variance of Terrestrial Heat Flow between the North American Craton and the Canadian Shield. *Geol. Soc. Am Bull* **85**, 519–522.

Springer J. S. (1985) Carbon in Archean rocks of the Abitibi belt (Ontario-Quebec) and its relation to gold distribution. *Can. J. Earth Sci.* **22**, 1945–1952.

Stolper D. A., Lawson M., Davis C. L., Ferreira A. A., Neto E. V. S., Ellis G. S., Lewan M. D., Martini A. M., Tang Y., Schoell M., Sessions A. L. and Eiler J. M. (2014a) Formation temperatures of thermogenic and biogenic methane. *Science* **344**, 1500–1503.

Stolper D. A., Sessions A. L., Ferreira A. A., Santos Neto E. V., Schimmelmann A., Shusta S. S., Valentine D. L. and Eiler J. M. (2014b) Combined 13C–D and D-D clumping in methane: Methods and preliminary results. *Geochim. Cosmochim. Acta* **126**, 169–191.

Stolper D. A., Martini A. M., Clog M., Douglas P. M., Shusta S. S., Valentine D. L., Sessions A. L. and Eiler J. M. (2015) Distinguishing and understanding thermogenic and biogenic sources of methane using multiply substituted isotopologues. *Geochim. Cosmochim. Acta* **161**, 219–247.

Taenzer L., Labidi J., Masterson A. L., Feng X., Rumble D., Young E. D. and Leavitt W. D. (2020) Low $\Delta^{12}CH_2D_2$ values in microbialgenic methane result from combinatorial isotope effects. *Geochim. Cosmochim. Acta* **285**, 225–236.

Telling J., Voglesonger K., Sutcliffe C. N., Lacrampe-Couloume G., Edwards E. and Sherwood Lollar B. (2018) Bioenergetic constraints on microbial hydrogen utilization in Precambrian deep crustal fracture fluids. *Geomicrobiol. J.* **35**, 108–119.

Thiagarajan N., Kitchen N., Xie H., Ponton C., Lawson M., Formolo M. and Eiler J. (2020a) Identifying thermogenic and microbial methane in deep water Gulf of Mexico Reservoirs. *Geochim. Cosmochim. Acta* **275**, 188–208.

Thiagarajan N., Xie H., Ponton C., Kitchen N., Peterson B., Lawson M., Formolo M., Xiao Y. and Eiler J. (2020b) Isotopic evidence for quasi-equilibrium chemistry in thermally mature natural gases. *Proc. Natl. Acad. Sci.* **117**, 3989–3995.

Thurston P. C., Ayer J. A., Goutier J. and Hamilton M. A. (2008) Depositional gaps in Abitibi greenstone belt stratigraphy: a key to exploration for syngenetic mineralization. *Econ. Geol.* **103**, 1097–1134.

Timmers P. H. A., Welte C. U., Koehorst J. J., Plugge C. M., Jetten M. S. M. and Stams A. J. M. (2017) Reverse methanogenesis and respiration in methanotrophic archaea. *Archaea.*

Trembath-Reichert E., Morono Y., Ijiri A., Hoshino T., Dawson K. S., Inagaki F. and Orphan V. J. (2017) Methyl-compound use and slow growth characterize microbial life in 2-km-deep sub-seafloor coal and shale beds. *Proc. Natl. Acad. Sci.* **114**, E9206–E9215.

Ventura G. T., Kenig F., Reddy C. M., Schieber J., Frysinger G. S., Nelson R. K., Dinel E., Gaines R. B. and Schaeffer P. (2007) Molecular evidence of Late Archean archaea and the presence of a subsurface hydrothermal biosphere. *Proc. Natl. Acad. Sci.* **104**, 14260–14265.

Vitale Brovarone A., Martinez I., Elmaleh A., Compagnoni R., Chaduteau C., Ferraris C. and Esteve I. (2017) Massive production of abiotic methane during subduction evidenced in metamorphosed ophicarbonates from the Italian Alps. *Nat. Commun.* **8**, 14134.

Wang D. T., Gruen D. S., Sherwood Lollar B., Hinrichs K.-U., Stewart L. C., Holden J. F., Hristov A. N., Pohlman J. W., Morrill P. L., Könneke M., Delwiche K. B., Reeves E. P., Sutcliffe C. N., Ritter D. J., Seewald J. S., McIntosh J. C., Hemond H. F., Kubo M. D., Cardace D., Hoehler T. M. and Ono S. (2015) Nonequilibrium clumped isotope signals in microbial methane. *Science* **348**, 428–431.

Wang D. T., Reeves E. P., McDermott J. M., Seewald J. S. and Ono S. (2018) Clumped isotopologue constraints on the origin of methane at seafloor hot springs. *Geochim. Cosmochim. Acta* **223**, 141–158.

Wang D. T., Welander P. V. and Ono S. (2016) Fractionation of the methane isotopologues $^{13}CH_4$, $^{12}C_H3D$, and $^{13}C_H3D$ during aerobic oxidation of methane by Methylococcus capsulatus (Bath). *Geochim. Cosmochim. Acta* **192**, 186–202.

Wang Z., Schauble E. A. and Eiler J. M. (2004) Equilibrium thermodynamics of multiply substituted isotopologues of molecular gases. *Geochim. Cosmochim. Acta* **68**, 4779–4797.

Ward J. A., Slater G. F., Moser D. P., Lin L. H., Lacrampe-Couloume G., Bonin A. S., Davidson M., Hall J. A., Mislowack B., Bellamy R. E. S., Onstott T. C. and Sherwood Lollar B. (2004) Microbial hydrocarbon gases in the Witwatersrand Basin, South Africa: Implications for the deep biosphere. *Geochim. Cosmochim. Acta* **68**, 3239–3250.

Warr O., Giunta T., Ballentine C. J. and Sherwood Lollar B. (2019) Mechanisms and rates of ^4He, ^{40}Ar, and H_2 production and accumulation in fracture fluids in Precambrian Shield environments. *Chem. Geol.* **530** 119322.

Warr O., Sherwood Lollar B., Fellowes J., Sutcliffe C. N., McDermott J. M., Holland G., Mabry J. C. and Ballentine C. J. (2018) Tracing ancient hydrogeological fracture network

age and compartmentalisation using noble gases. *Geochim. Cosmochim. Acta* **222**, 340–362.

Webb M. A. and Miller T. F. (2014) Position-Specific and Clumped Stable Isotope Studies: Comparison of the Urey and Path-Integral Approaches for Carbon Dioxide, Nitrous Oxide, Methane, and Propane. *J. Phys. Chem. A* **118**, 467–474.

Wei L., Schimmelmann A., Mastalerz M., Lahann R. W., Sauer P. E., Drobniak A., Strąpoć D. and Mango F. D. (2018) Catalytic generation of methane at 60–100 °C and 0.1–300 MPa from source rocks containing kerogen Types I, II, and III. *Geochim. Cosmochim. Acta* **231**, 88–116.

Wellmer E.-W., Berner U., Hufnagel H. and Wehner H. (1999) Carbon Isotope Geochemistry of Archean Carbonaceous Horizons in the Timmins Area. In *(2019) Economic Geology Monograph 10: The Giant Kidd Creek Volcanogenic Massive Sulfide Deposit, Western Abitibi Subprovince, Canada* (eds. M. D. Hannington and C. T. Barrie). The Economic Geology Publishing Co, pp. 441–456.

Whiticar M. J. (1999) Carbon and hydrogen isotope systematics of bacterial formation and oxidation of methane. *Chem. Geol.* **161**, 291–314.

Whiticar M. J., Faber E. and Schoell M. (1986) Biogenic methane formation in marine and freshwater environments: CO_2 reduction vs. acetate fermentation - Isotope evidence. *Geochim. Cosmochim. Acta* **50**, 693–709.

Xia X. and Gao Y. (2019) Kinetic clumped isotope fractionation during the thermal generation and hydrogen exchange of methane. *Geochim. Cosmochim. Acta* **113**, 115–123.

Yoshinaga M. Y., Holler T., Goldhammer T., Wegener G., Pohlman J. W., Brunner B., Kuypers M. M. M., Hinrichs K. U. and Elvert M. (2014) Carbon isotope equilibration during sulphate-limited anaerobic oxidation of methane. *Nat. Geosci.* **7**, 190–194.

Young E. D. (2019) A two-dimensional perspective on CH4 isotope clumping. In B. Orcutt, I. aniel, R. Dasgupta (Eds.) (2019) Deep Carbon: Past to Present. Cambridge, UK: Cambridge University Press doi: 10.1017/9781108677950.

Young E. D., Kohl I. E., Sherwood Lollar B., Etiope G., Rumble D., Li (李姝宁) S., Haghnegahdar M. A., Schauble E. A., McCain K. A., Foustoukos D. I., Sutclife C., Warr O., Ballentine C. J., Onstott T. C., Hosgormez H., Neubeck A., Marques J. M., Pérez-Rodríguez I., Rowe A. R., LaRowe D. E., Magnabosco C., Yeung L. Y., Ash J. L., Bryndzia L. T., Rumble III D., Li (李姝宁) S., Haghnegahdar M. A., Schauble E. A., McCain K. A., Foustoukos D. I., Sutclife C., Warr O., Ballentine C. J., Onstott T. C., Hosgormez H., Neubeck A., Marques J. M., Pérez-Rodríguez I., Rowe A. R., LaRowe D. E., Magnabosco C., Yeung L. Y., Ash J. L. and Bryndzia L. T. (2017) The relative abundances of resolved l2CH2D2 and 13CH3D and mechanisms controlling isotopic bond ordering in abiotic and biotic methane gases. Geochim. Cosmochim. Acta 203, 235–264.

Young E. D., Rumble D., Freedman P. and Mills M. (2016) A large-radius high-mass-resolution multiple-collector isotope ratio mass spectrometer for analysis of rare isotopologues of O_2, N_2, CH_4 and other gases. *Int. J. Mass Spectrom.* **401**, 1–10.

Associate editor: Shuhei Ono